

# One-shot learning of paired association navigation with biologically plausible schemas

M Ganesh Kumar<sup>1,2,3,4</sup>, Cheston Tan<sup>4</sup>, Camilo Libedinsky<sup>1,2,5,6</sup>, Shih-Cheng Yen<sup>1,2,3</sup>, Andrew Y. Y. Tan<sup>7,8,9,10</sup>

1. Integrative Sciences and Engineering Programme, NUS Graduate School, National University of Singapore
2. The N.1 Institute for Health, National University of Singapore
3. Engineering Design and Innovation Centre, College of Design and Engineering, National University of Singapore
4. Centre for Frontier AI Research, Agency for Science, Technology and Research
5. Department of Psychology, National University of Singapore
6. Institute of Molecular and Cell Biology, Agency for Science, Technology and Research
7. Department of Physiology, Yong Loo Lin School of Medicine, National University of Singapore
8. Healthy Longevity Translational Research Programme, Yong Loo Lin School of Medicine, National University of Singapore
9. Cardiovascular Disease Translational Research Programme, Yong Loo Lin School of Medicine, National University of Singapore
10. Neurobiology Programme, Life Sciences Institute, National University of Singapore

Correspondence: M Ganesh Kumar ([m\\_ganeshkumar@u.nus.edu](mailto:m_ganeshkumar@u.nus.edu)), Andrew Tan ([atyy@alum.mit.edu](mailto:atyy@alum.mit.edu))

## Abstract

Schemas are knowledge structures that can enable rapid learning. Rodent one-shot learning in a multiple paired association navigation task has been postulated to be schema-dependent. But how schemas, conceptualized at Marr's computational level, correspond with neural implementations remains poorly understood, and a biologically plausible computational model of the rodent learning has not been demonstrated. Here, we compose such an agent from schemas with biologically plausible neural implementations. The agent contains an associative memory that can form one-shot associations between sensory cues and goal coordinates, implemented with a feedforward layer or a reservoir of recurrently connected neurons whose plastic output weights are governed by a novel 4-factor reward-modulated Exploratory Hebbian (EH) rule. Adding an actor-critic allows the agent to succeed even if an obstacle prevents direct heading. With the addition of working memory, the rodent behavior is replicated. Temporal-difference learning of a working memory gating mechanism enables one-shot learning despite distractors.

Keywords: one-shot learning, schema, Hebbian plasticity, reinforcement learning

## Introduction

Schemas are knowledge structures or frameworks that describe relationships among information and actions (Rumelhart, 1980; Rumelhart & Ortony, 1977). Importantly, schemas can aid rapid learning (Bartlett & Burt, 1932). For example, one often better recalls content from a lecture on a subject in which one already has a framework for understanding. To make the biological mechanisms of schema-dependent learning accessible to investigation with the techniques of experimental neuroscience, Tse and colleagues devised a behavioral paradigm in which rodents demonstrated rapid learning after an initial gradual learning experience, like that displayed by people during schema-dependent learning (Tse et al, 2007). Rodents performed a two-stage multiple paired associations (MPA) task. In the first stage, rodents were given a cue at the start of each trial, indicating where they had to go to get a reward. Different cues were presented on different trials, and rodents learned to associate different cues with the corresponding target locations. Learning was relatively slow in the first stage. In the second stage, new cues were given, and learning was rapid with rodents demonstrating one-shot learning, needing only a single exposure to each new cue to navigate to the correct location on subsequently encountering the cue. Schema construction in the first stage was proposed to have enabled the one-shot learning in the second stage.

Machine learning algorithms from fields like transfer learning and meta-learning behave similarly, with prior learning accelerating subsequent learning to the point of being few-shot or one-shot (Finn et al.,

2017; Hospedales et al., 2021; Ravi & Larochelle, 2017; Ritter et al., 2018; Wang et al., 2018). Such algorithms have been adapted for modelling scenarios resembling the experimental paradigm of Tse and colleagues (Hwu & Krichmar, 2020; McClelland, 2013). However, those models depend on backpropagation or contrastive Hebbian learning, which are not biologically plausible, as synaptic plasticity in backpropagation is acausal or nonlocal, while contrastive Hebbian learning depends on synaptic rules that differ in alternating phases (Bellec et al., 2020; Lillicrap et al., 2020; Murray, 2019). Furthermore, what a schema is has not been concretely conceptualized. Hence, schemas, their role in enabling one-shot learning, and their biologically plausible implementation remains unclear.

To address these issues, we describe schemas that could underlie the observed rodent behavior in conceptual terms roughly corresponding to Marr's computational level, outline symbolic or machine learning algorithms that could perform the computations, and explain how each schema has a corresponding biologically plausible implementation (Marr, 2010; Marr & Poggio, 1977; Poggio, 2012). We compose these schemas into a fully neural network-based agent in which synaptic plasticity is governed by biologically-plausible rules, and that replicates the one-shot learning of rodents.

We build on work by Foster and colleagues (2000), who demonstrated a biologically-plausible agent that modelled rodent one-shot learning of a delayed matching-to-place (DMP) task. In the DMP task, rats are required to navigate to a target whose position remains the same throughout four trials each day, but whose position is changed every day. During the first few days, the time taken to find the newly displaced target gradually decreases from trial to trial, but after several days, rats rapidly find the target after one trial (Steele & Morris, 1999). Foster and colleagues' agent may be thought of as composed of 3 schemas. (1) LEARN METRIC REPRESENTATION allows the agent to self-localize by learning coordinates that are a continuous metric representation of its current position in the environment. This schema was neurally implemented with biologically plausible synaptic plasticity involving a path integration temporal difference (TD) error. (2) LEARN GOAL COORDINATES allows the agent to learn the goal coordinates in one shot. This schema had a non-neural, symbolic implementation that stores the target coordinates at which a reward was disbursed. (3) NAVIGATE allows the agent to perform vector subtraction between coordinates of its current and goal locations to obtain a direction in which to head to reach the goal. This schema also had a non-neural, symbolic implementation. This agent shows gradual learning before transitioning to one-shot learning because it executes 2 learning schemas: LEARN METRIC REPRESENTATION learns slowly while LEARN GOAL COORDINATES learns in one shot. Initial learning is gradual as it involves both the schemas, but then becomes one shot once LEARN METRIC REPRESENTATION has completed learning and new learning depends only on LEARN GOAL COORDINATES.

Because the LEARN GOAL COORDINATES schema is a non-associative memory that stores the coordinates of a single goal, the agent of Foster and colleagues is unable to learn the MPA task. We therefore replaced the symbolic memory implementation with the LEARN FLAVOR-LOCATION schema, which is an associative memory that is able to learn each of several multiple cue-location paired associations in one shot.

We demonstrate two agents in which the LEARN GOAL COORDINATES schema is replaced with the LEARN FLAVOR-LOCATION schema, enabling one-shot learning in both DMP and MPA tasks. One of the agents is symbolic, while the other is neural. In both symbolic and neural agents, LEARN METRIC REPRESENTATION is neurally implemented similar to Foster and colleagues. The symbolic agent implements LEARN FLAVOR-LOCATION symbolically with a key-value matrix to store and recall cue-associated goal coordinates. NAVIGATE is symbolically implemented as by Foster and colleagues. The neural agent implements LEARN FLAVOR-LOCATION with either a nonlinear feedforward layer or a reservoir of recurrently connected units whose readout weights undergo synaptic plasticity governed by a novel biologically-plausible 4-factor Exploratory Hebbian (EH) learning rule to learn a flavor-location association after one trial. For the neural agent, NAVIGATE is neurally implemented by using backpropagation to train a network whose input-output relationships closely match those of the symbolic NAVIGATE implementation. As backpropagation is not biologically plausible, we assume that the neural implementation of NAVIGATE arises via processes during development or prior experience that we do not model. When these agents are supplemented with an

actor-critic, they can demonstrate one-shot learning of new associations even in an arena with an obstacle. Lastly, we show that the agent can be given working memory so that it demonstrates one-shot learning even if the cue is available only at the start of a trial. If the agent uses a reward prediction error to learn a working memory gating policy, one-shot learning with a transient initial cue is possible even if distractor stimuli are present during navigation.

## Results

We begin by describing three schemas: LEARN METRIC REPRESENTATION, LEARN FLAVOR-LOCATION and NAVIGATE. For each, we give a conceptual description roughly corresponding to Marr's computational level, outline a symbolic or machine learning algorithm for the computation, and show how the schema can be implemented using neural networks and biologically plausible learning rules. We then construct 3 basic agents: the symbolic and the neural agents are composed from the schemas, while the actor-critic agent is not schema-based. We study all basic agents in the DMP task. We further study the basic agents and 2 hybrid schema-actor-critic agents in navigation past an obstacle to a single goal. The core of this paper studies all basic agents in the two stage-MPA task. We further study the basic agents and the hybrid agents in a version of the MPA task with an obstacle. The schema agents, but not the actor-critic, succeed at one-shot learning in the DMP and MPA tasks while the hybrid agents are needed for the tasks with an obstacle. Finally, we demonstrate that working memory and, learning of a gating policy that selects for task relevant cues and filters out distractor cues, can be incorporated into the neural schema-actor-critic agent.

A) LEARN METRIC REPRESENTATION SCHEMA: Learn a metric representation of the environment to self-localize and for NAVIGATE		
<b>Computation</b> Use self-motion information and place cell activity to learn a continuous X–Y coordinates–based metric representation for vector–based navigation.	<b>Neural implementation</b> Place cells are used as input to the X and Y coordinate cells (Eq. 18) as outputs. The synapses from place cells to coordinate cells are gradually learned using a path integration temporal difference error (Eq. 21) modulated learning rule (Eq. 23) with eligibility trace (Eq. 22).	
<b>Algorithm</b> Estimate start coordinates $p(0) = (0,0)$ for $t < T$ : Move in direction specified by policy Estimate coordinates using place cells Compute path integration error Compile history of place cell activity Minimise path integration error end	$\tau \dot{p}_i(t) = -p_i(t) + \sum_{j=1}^p W_{ij}^{coord} u_j^{pc}(t) + \sqrt{\tau \sigma_{coord}^2} \xi(t) \quad (18)$ $\delta_i^{coord}(t) = p_i(t) - p_i(t - \Delta t) - \hat{a}_i(t) \quad (21)$ $\tau_{coord} \dot{e}_j(t) = -e_j(t) + u_j^{pc}(t) \quad (22)$ $\Delta W_{ij}^{coord}(t) \propto e_j(t) \cdot \delta_i^{coord}(t) \quad (23)$	
B) LEARN FLAVOR–LOCATION SCHEMA: Associate flavor cue to reward location after one trial to recall goal for NAVIGATE		
<b>Computation</b> Associate the flavor cue with the coordinates at which a reward was disbursed after a single trial. Use flavor cues to recall the goal coordinates.	<b>Neural implementation</b> The cue vector is passed as input to a feedforward layer or reservoir with three output units representing X, Y goal coordinates and reward recall value (Eq. 28). Only the output synapses are subject to the reward modulated Exploratory Hebbian rule (Eq. 30). Associations are depressed using acetylcholine modulated Hebbian learning (Eq. 35).	
<b>Algorithm</b> Initialize associative memory and get cue for $t < T$ : Use cue to query the keys to recall the associated goal coordinates and reward value from the value matrix if recalled reward value > threshold then Navigate to goal using NAVIGATE if no reward at goal then Delete flavor–location association else Explore maze using default policy if reward disbursed then Store flavor cue in key matrix and agent's coordinates estimated using metric representation and transformed reward in value matrix end	$g_i^{noisy}(t) = \sum_{j=1}^N W_{ij}^{goal} \eta_j(t) + \sqrt{\tau \sigma_{goal}^2} \xi(t) \quad (27)$ $g_i^*(t) = [p_i(t), \Theta(R(t))] \quad (28)$ $\Delta W_{ij}^{goal}(t) \propto r_j(t) \cdot (g_i^{noisy}(t) - g_i(t)) \cdot M(t) \cdot \Theta[R(t)] \quad (30)$ $M(t) = \begin{cases} 1, & \bar{P}(t) < P(t) \\ 0, & otherwise \end{cases} \quad (31)$ $P(t) = -\sum_{i=1}^3 [g_i^*(t) - g_i^{noisy}(t)]^2 \quad (32)$ $\Delta W_{ij}^{goal}(t) \propto r_j(t) \cdot g_i(t) \cdot -\Omega_{Ach} \quad (35)$	
C) NAVIGATE SCHEMA: Move from arbitrary location to goal location		
<b>Computation</b> Take in agent's current coordinates, recalled goal coordinates and reward recall value as input to output direction to move.	<b>Neural implementation</b> Neural network with two nonlinear hidden layers was pre-trained by backpropagation on a dataset with different current coordinate, goal coordinate, reward recall values and action. Weights were fixed during task learning.	
<b>Algorithm</b> Get agent's current coordinates $p(t)$ Get goal coordinates $g(t)$ and transformed reward for $t < T$ : if recalled reward > threshold (Eq. 38), then Compute vector subtraction between current and goal coordinates (Eq. 36) Choose action based on direction specified by vector (Eq. 37) else No action selected end	$d_{j \in \{x,y\}}(t) = g_{j \in \{x,y\}}(t) - p_j(t) \quad (36)$ $d_t^{NAV}(t) = \text{softmax} \left( \sum_{j=1}^M K_i^{actions} d_j \right) \cdot \varepsilon(t) \quad (37)$ $\varepsilon(t) = \begin{cases} 1, & 0.6 < g_{j=3}(t) \\ 0, & otherwise \end{cases} \quad (38)$	

**Figure 1. Schemas for learning one-shot navigation to multiple goals.** A schema is a framework that describes relationships between information and actions. Each row summarizes a schema conceptualized as a computation in Marr's sense, with a corresponding algorithm (left), and key equations (center) and connectivity schematic (right) of a biologically plausible neural implementation.

## Schemas for one-shot navigation to multiple goals

Marr proposed that we can understand the brain's information processing at 3 levels: computation, algorithm, and implementation (Marr, 2010; Marr & Poggio, 1977; Poggio, 2012). The computation specifies the input and desired output or goal; the algorithm is pseudocode that carries out the computation; the implementation are physical and biological processes that exactly or approximately realize the computation and algorithm. Here we introduce 3 schemas, which we will subsequently use to compose agents. For each schema, we give a conceptualization as a computation in Marr's sense, outline a symbolic or machine learning algorithm, and describe a biologically plausible neural implementation (Fig. 1).

### LEARN METRIC REPRESENTATION schema

LEARN METRIC REPRESENTATION is a schema whose computation is to learn a continuous metric representation of an agent's position (Fig. 1A). This computation enables an agent to learn to use self-motion information and the place cell representation of its own position to output its own X and Y coordinates, which are a continuous metric representation of position. The continuous metric representation can then be used by the NAVIGATE schema to compute a vector from the agent's position to the goal. This conversion between position representations is needed because place cell or grid cells represent an agent's position, but that representation is insufficient or inconvenient for computing a vector from the agent's position to the goal (Bush et al., 2015; Fiete et al., 2008; Moser et al., 2008).

LEARN METRIC REPRESENTATION's algorithm has a biologically plausible neural implementation, so we describe that directly (refer to Fig. 1A for the pseudocode). A layer of place cells makes feedforward projections onto X and Y coordinate neurons (Eq. 18). The agent computes a path integration temporal difference (TD) error  $\delta_{i \in \{x,y\}}^{coord}(t)$  for the X and Y coordinates by comparing its self-motion with the difference between its current and previous estimated coordinates (Eq. 21). Plasticity of the feedforward projections depends on an eligibility trace representing presynaptic place cell activity (Eq. 22), with the eligibility trace modulated by the path integration TD error (Eq. 23) (Foster et al., 2000).

As the agent moves randomly around the arena, the path integration TD error is gradually minimized (Supplementary Fig. 1A) till the synaptic weights from the place cells to X and Y coordinate cells converge to a stable representation, such that the moving left to right or bottom to top causes linear increases in the firing rate of the X or Y coordinate cells respectively (Fig. 2A top). This results in increasing similarity between the agent's estimate of its position coordinates and the correct position coordinates for arbitrary agent paths (Fig. 2A bottom).

### LEARN FLAVOR-LOCATION schema

LEARN FLAVOR-LOCATION is a schema whose computation is to associate a flavor cue with the goal coordinates after a single successful trial (Fig. 1B). In a successful trial, an agent reaches the goal corresponding to the cue, and reward is received at the goal. As the goal coordinates are those where the agent is rewarded, reward is used to gate the association of flavor cues and goal coordinates.

A symbolic algorithm for LEARN FLAVOR-LOCATION stores the flavor cue in the key matrix, and the goal coordinates and a reward recall value in the value matrix after a single successful trial (Fig. 2B). In a subsequent trial, the flavor cue is treated as a query, and a distance-based metric (Eq. 24) is used to compare the query against the key matrix to identify the memory index, which is used to recall goal coordinates from the value matrix (Eq. 25). If recall is accurate, the reward recall value will be close to 1; if recall is inaccurate, the reward recall value will be closer to 0. When the agent navigates to the recalled goal coordinates but no reward is disbursed, or when the trial ends without reward, the association is deleted by setting the flavor cue, goal coordinates and reward recall value at that memory index to zero (Cue 8 in Fig. 2B). When the same cue occurs in a subsequent trial, the reward recall value will be close to 0, and the agent switches to exploring the arena. This way, a key-value matrix allows

for writing and deleting specific flavor–location associations after a trial without disrupting other associations.

A biologically plausible neural implementation for LEARN FLAVOR-LOCATION consists of a nonlinear feedforward layer or a reservoir of recurrently connected neurons with three goal neurons that represent the goal coordinates and reward recall value (Eq. 27). The flavor cue is given as an input to the network using synaptic weights drawn from a random uniform distribution. The synapses from the feedforward layer or the reservoir to the goal neurons can be trained by the reward modulated least mean squares FORCE (LMS) algorithm (Eq. 29) (Hoerzer et al., 2012; Sussillo & Abbott, 2009), or a more biologically plausible novel 4-factor reward-modulated EH rule (Eq. 30) adapted from Hoerzer and colleagues (2012).

The first two factors of the latter rule contains the presynaptic factor involving the feedforward or reservoir activity, and the postsynaptic factor involving goal neuron activity. The third factor  $M(t)$  is a binary variable that coarsely indicates whether the goal neurons  $g(t)$  are getting closer to or further from their estimated target vector  $g^*(t)$ . The estimated target vector is a concatenation of the agent’s current coordinates and the reward recall value (Eq. 28). The fourth factor is also a binary variable that indicates the presence or absence of a reward, and is crucial to ensure that the association between the flavor cue and agent’s current coordinates is learned only when a reward is disbursed.

To study the neural implementation of LEARN FLAVOR-LOCATION alone (without being composed with other schemas), we switched on plasticity as if reward was constantly received for the results in Fig. 2C. Networks with the feedforward layer (FF) or reservoir (Res) with three goal neurons were trained to learn one to 200 cue-coordinate associations for one trial. In the subsequent trial, the same cues were given as input to test the recall error of the goal coordinates and the reward recall value. Both the LMS and EH rules were used. Learning rates were the same across hyperparameters.

When the feedforward layer or reservoir consisting of 128 neurons and fully-connected synapses were trained using the EH rule, the former demonstrated a significantly lower recall mean squared error (MSE) compared to the latter after one trial of learning (AUC t-test  $t = -10.7, p < 10^{-4}$ ). An even lower recall MSE was achieved when either a feedforward layer (AUC t-test  $t = -7.67, p < 10^{-4}$ ) or reservoir (AUC t-test  $t = -16.1, p < 10^{-4}$ ) with 128 units were trained using the LMS rule for up to 107 association pairs (refer to Supplementary Fig. 2). However, the recall MSE increased monotonically with the number of associations such that the feedforward network trained by the EH rule achieved a lower MSE when recalling more than 107 associations (AUC t-test  $t = -11.1, p < 10^{-4}$ ).

When the number of neurons in the feedforward layer or reservoir were increased from 128 to 1024 units, the recall MSE decreased significantly for both (Fig. 2C and Supplementary Fig. 2). With 1024 units, the reservoir achieved a significantly lower MSE compared to the feedforward layer when recalling 1 to 200 associations (AUC t-test  $t = -25.7, p < 10^{-4}$ ). Interestingly, both the feedforward layer (AUC t-test  $t = -0.643, p = 0.523$ ) and reservoir (AUC t-test  $t = -0.338, p = 0.737$ ) achieved similar recall MSE when trained by either the LMS or EH rule, consistent with the learning performance observed by Hoerzer et al. (2012). However, this trend did not hold when smaller networks were trained using either the LMS or EH rule (Supplementary Fig. 2).

Hence, the one-shot association capacity depends on the network architecture, number of neurons, and the learning rule. Moreover, we did not observe catastrophic forgetting in these associative networks, which may differ from Hopfield networks in this respect. Instead, these networks demonstrate a monotonic increase in recall MSE indicating smooth association capacity–accuracy tradeoff like other recent hetero-associative networks (Sharma et al., 2022; Tyulmankov et al., 2021).

It is also possible to delete a specific cue-coordinate association, as the key-value matrix algorithm could, with biologically plausible synaptic plasticity. To do so, we introduce synaptic depression governed by a previously proposed 3-factor acetylcholine-modulated Hebbian rule (Eq. 35) (Brzosko et al., 2017; Zannone et al., 2018). Figure 2D shows that when the associative EH rule was switched on (red dashed line) for a reservoir to learn cue-coordinate association, the readout units converged to specific X (blue trace), Y (orange trace) coordinates and a reward recall value of 1 (green trace) within

4 seconds, which were maintained after plasticity was switched off (black dashed line). When the reservoir was reset with random activity and the same cue was presented, the readout units recalled the associated goal coordinates and the reward recall value was close to 1.

When different amounts of acetylcholine were introduced ( $Ach = 0.1, 0.01, 0.001$ ) for five seconds (magenta to black dashed lines) for Cues 1, 2 and 3, the activity of the three readout units converged towards zero at different rates, representing deletion of cue–coordinate association. Specifically, acetylcholine at levels 0.1, 0.01 and 0.001 need to be introduced for 1, 7, and 45 seconds so that there will be sufficient time for synaptic depression to cause the reward recall value (green trace) to fall below the 0.6 threshold, or 3, 18, and 160 seconds to fall below 0.1, respectively. Importantly, deleting cue specific associations did not affect the recall of other cue–coordinate associations (Fig. 2D, Cue 4) demonstrating the network’s ability to write and delete paired associations without disrupting other associations.

As there is increased cholinergic tone during exploratory behavior, synaptic depression governed by 3-factor acetylcholine-modulated Hebbian plasticity has been modelled as being persistently on during exploration (Brzosko et al., 2017; Zannone et al., 2018). Likewise, synaptic plasticity in LEARN FLAVOR-LOCATION is solely due to 3-factor acetylcholine-modulated Hebbian plasticity (Refer to Table 1), except when reward disbursement triggers reward-modulated exploratory Hebbian learning.

### **NAVIGATE schema**

NAVIGATE is a schema whose computation allows the agent to head directly to a recalled goal coordinate from any location, even if it had not traversed that path. It can be performed by a 3 step algorithm: (1) vector subtraction (Eq. 36) between the goal and current coordinates to determine the distance and direction to the goal from the current location (2) choose the relevant action (Eq. 37) out of all possible actions that will bring the agent closer to the goal via direct heading and (3) suppress the chosen action (Eq. 38) if the recalled reward value falls below a threshold value of 0.6 (Fig. 1C). Vector subtraction and the corresponding action is chosen only if the recalled reward value is greater than a threshold value of 0.6. If the recalled reward value falls below the threshold, the output vector is suppressed by returning a zero vector, without specifying the direction of movement.

To obtain a neural implementation of NAVIGATE, we pretrained a network with two nonlinear hidden layers, each with 128 units using backpropagation on a dataset comprising different current coordinates, goal coordinates and reward recall values as inputs and the relevant action to take, computed symbolically (Eq. 36–38) as outputs (refer to Methods). The network weights were fixed throughout the DMP and MPA tasks (purple arrows in Fig. 1C and Fig. 3A).

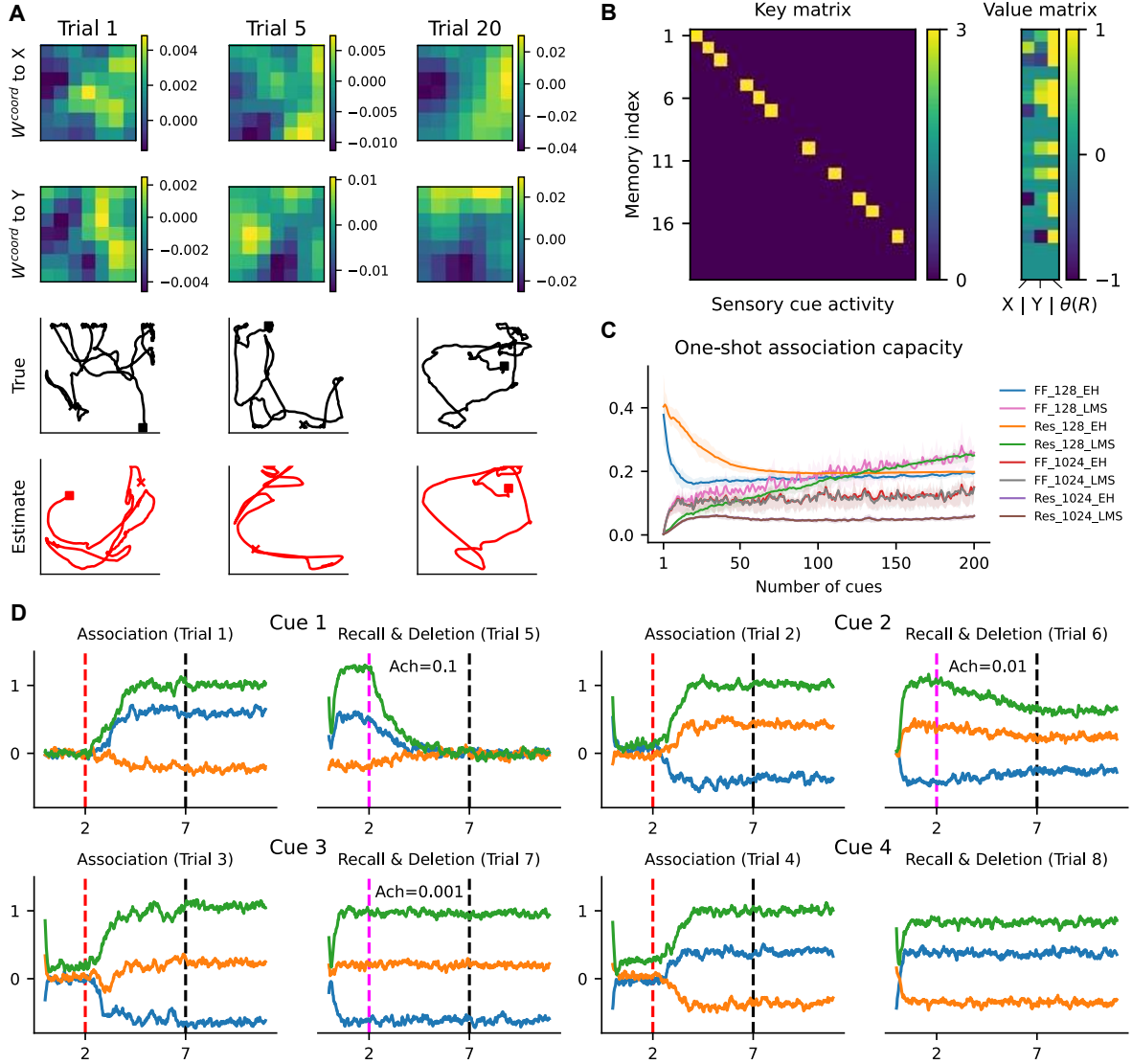


**Figure 2. Representations learned using LEARN METRIC REPRESENTATION or LEARN FLAVOR-LOCATION schemas.** A) As LEARN METRIC REPRESENTATION (as shown in Fig. 1A) moves randomly in an arena, the synaptic weights from 49 place cells to the X and Y coordinate cells converge to a stable representation, such that an agent moving left to right or bottom to top causes linear increases in the firing rate of the X or Y coordinate cells respectively (top). This results in increasing similarity between the agent’s true and estimated position coordinates (bottom). B) The symbolic LEARN FLAVOR-LOCATION algorithm uses a key-value matrix to store the cue vector in each row of the key matrix and the value matrix stores the X, Y goal coordinates (between  $-1$  to  $1$ ) and reward recall value (between  $0$  to  $1$ ). A distance metric is used to recall cue associated goal coordinates. C) To study the neural implementation of LEARN FLAVOR-LOCATION alone (without being composed with other schemas), plasticity was always on as if reward was being received. The feedforward layer or reservoir could store and recall up to 200 cue–coordinate associations after a single trial, while showing smooth capacity–accuracy tradeoff. Increasing the size of the network decreased the recall mean squared error (MSE). A reservoir with 1024 units trained using the EH rule (purple) achieved similar recall MSE as when trained using the more powerful but biologically implausible LMS rule (brown). The small differences between the purple and brown curves might not be visible. The shaded area indicates 25th and 75th quantiles. D) Each of the 4 cue–coordinate associations were stored sequentially across 4 trials in a neural implementation of LEARN FLAVOR-LOCATION with a reservoir; this was followed by sequential recall and deletion of each cue in 4 more trials. Each panel shows the activity of goal neurons (X coordinate – blue, Y coordinate – orange, reward recall value – green) corresponding to association, recall and deletion of a particular cue. During association, the EH rule was switched on as if reward was being received for 4.5 seconds (red dashed line to black dashed line) to associate a cue with a pair of randomly chosen coordinates. Thereafter plasticity was switched off and the goal neurons maintained the activity. During recall and deletion, reservoir activity was reinitialized and a cue

subsequently given, the network recalled the associated coordinate. Acetylcholine-modulated Hebbian learning rule was switched on (magenta dashed line to black dashed line) to induce synaptic depression. In each panel, a different value of acetylcholine was used. Higher acetylcholine values increased the rate of synaptic depression resulting in the deletion of cue-specific associations. The sequential deletion of associations for Cues 1 to 3 did not affect accurate recall of Cue 4 coordinates.

## One-shot learning of a single displaced goal

We begin by checking whether a symbolic agent, a neural agent composed from the schemas described above, and an actor-critic agent that uses trial-and-error for reinforcement learning and is not schema-based (Kumar et al., 2022) can learn to navigate to a goal that is displaced every five trials, with the fifth trial being an unrewarded probe lasting 60 seconds. In each trial, the agent starts at a randomly chosen midpoint at the arena boundary and receives the same sensory cue (e.g. Sensory Cue 1) till it reaches the reward location. The same cue is given to the agent despite target displacement to evaluate the ability to unlearn the previous target and relearn the new goal location. This unlearning and relearning task is harder compared to learning distinct policies for different sensory cues as evaluated in Kumar et al. (2022).

All agents have leaky rate-based neurons and receive input from place cells encoding position, and the sensory cue. They have an actor that is a ring of neurons whose output dictates the speed and direction of agents. The actor-critic agent (Fig. 3A, left) has an additional critic output that learns a value function to compute the TD error (Eq. 15). Only the synapses from the reservoir to the actor and the critic are subject to TD error-modulated Hebbian plasticity (see Methods).

Both the symbolic and the neural schema agents learn X-Y coordinate representations of their position via path integration TD error-modulated Hebbian plasticity in the neural implementation of LEARN METRIC REPRESENTATION.

The symbolic agent (Fig. 3A, middle) uses the symbolic algorithm for LEAN FLAVOR-LOCATION to associate the sensory cue with the goal coordinates by storing the sensory cue in the Key Matrix and the coordinates at which the reward was disbursed and the transformed reward at the corresponding memory index in the Value Matrix. In a subsequent trial, the sensory cue is treated as a query and a distance metric identifies the memory index with the highest similarity in the Key Matrix (Eq. 24). The memory index is used to recall the corresponding goal coordinate from the Value Matrix (Eq. 25). The agent’s current coordinates and recalled goal coordinates are passed to the symbolic NAVIGATE schema, which performs vector subtraction to determine the goal vector (Eq. 36) and chooses an action for movement in the direction of the goal vector (Eq. 37). This direction information is passed to the actor if the reward recall value is greater than a threshold value of 0.6 (Eq. 38).

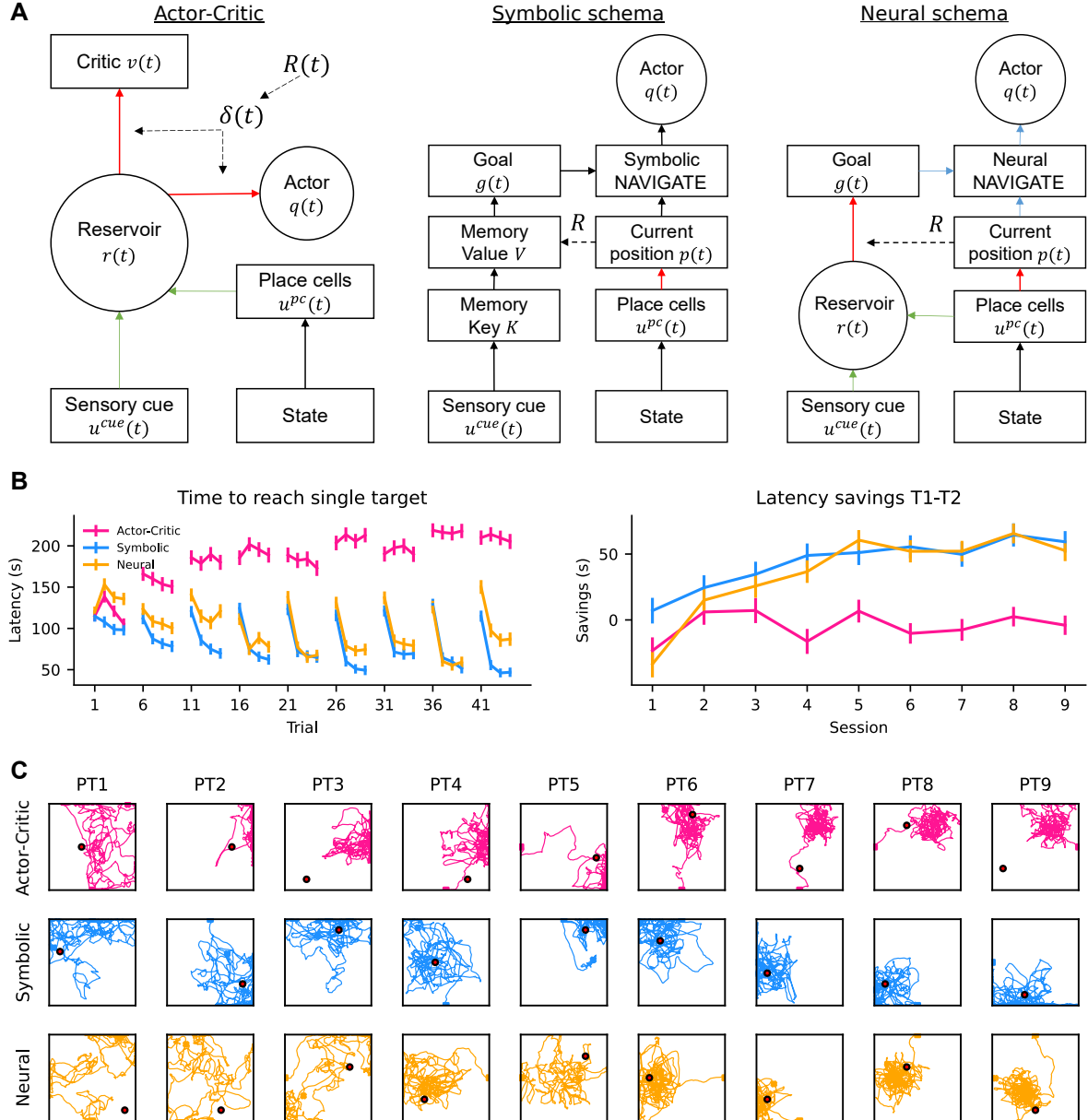
Like the symbolic agent, the neural agent (Fig. 3A, right) is composed from the three schemas, but with neural implementations of LEARN FLAVOR-LOCATION and NAVIGATE. LEARN FLAVOR-LOCATION was implemented with a reservoir whose synapses onto the goal neurons were subject to 4-factor reward-modulated EH plasticity (Eq. 30). The target is a concatenated vector comprising the agent’s current coordinates and the reward recall value (Eq. 28). The synapses are also persistently modified by the acetylcholine-modulated Hebbian rule that causes synaptic depression resulting in gradual decay of activity representing recalled goal information (Fig. 2D and Methods). The reward-modulated EH rule updates the synapses such that presentation of the cue causes the goal neurons to recall the coordinates at which reward was received. The recalled goal coordinates and the agent’s current coordinates are inputs to NAVIGATE, implemented as a neural network pretrained to output the distance and direction of movement, which is then passed to the actor.

Figure 3B shows that the actor-critic agent gradually learned to navigate to the single goal in the first session (Trials 1 to 4), but the latency increased after every goal displacement and plateaued within each session. Our actor-critic agent with a reservoir layer replicates the same stunted behaviour of a simplified actor-critic agent observed in Foster et al. (2000). Importantly, the Actor-Critic did not show a significant decrease in latency between the first and second trials for any sessions ( $t < 1.52, p > 0.13$ ), failing to demonstrate one-shot learning.

In contrast, the symbolic and neural schema agents demonstrated one-shot learning of displaced targets as shown by a latency decrease between the first and second trials that became increasingly apparent after Session 4 (Trial 16 in Fig. 3B left). Both agents achieved similar latency savings (Fig. 3B right) since Session 2 till Session 9 with Session 3 having the largest but insignificant difference in savings ( $t = -1.93, p = 0.0545$ ). While in Session 1, the Neural agent showed significantly lower savings compared to the Symbolic agent ( $t = -5.67, p < 10^{-4}$ ) but comparable savings to the Actor-Critic ( $t = 1.4, p = 0.162$ ).

The average latency decrease from Session 5 to 9 was  $-2.5 \pm 8$  s for the Actor-Critic,  $56 \pm 9$  s for symbolic, and  $57 \pm 8$  s for neural agents (see right plot in Fig. 3B). One-shot learning emerged as the schema agents gradually learned the metric representation while immediately learning the goal coordinates after each trial.

Figure 3C shows example agent trajectories during the non-rewarded probe trial, which took place after the 4th trial of each session. The actor-critic agent's policy converges erroneously to navigating to the prior learned goal location instead of new goal locations despite target displacement. This is because the synaptic weights are incrementally updated to converge to a particular value and policy map, and becomes less adaptable with prolonged training. The symbolic and the neural agents initially show indirect trajectories, but directness of navigation to the goal improves, becoming apparent from around PT4.



**Figure 3. One-shot learning of delayed match to place (DMP) task by schema agents.** A) Architectures of actor-critic (left), symbolic schema (center), and neural schema (right) agents. Synapses from the reservoir to the actor and critic were learned using forms of TD error-modulated plasticity. The red, green and blue arrows indicate synaptic weights updated using biologically plausible learning rules, drawn from a random uniform distribution and pretrained using backpropagation respectively. In both symbolic and neural agents, synapses from place cells to coordinate cells were learned via path integration TD error-modulated Hebbian plasticity. The symbolic agent used a symbolic key-value associative memory system. The neural agent used a reservoir with synapses to goal neurons trained using reward-modulated EH plasticity to store and recall goal coordinates. For the DMP task, all agents received the same Cue 1 throughout the trial for all trials, and navigated to a single target that is displaced every 5 trials, with the last trial being an unrewarded probe lasting for 60 seconds. B) Latency (left) to reach target, and difference in latency between Trials 1 and 2 (right). The actor-critic agent initially learns to navigate to single targets, but learning worsens as trials progress. Both the symbolic and the neural schema agents show one-shot learning of displaced targets that is increasingly apparent from about Session 4. There are 720 simulations per agent. Error bars indicate 95% confidence intervals. C) Each row shows example trajectories of an agent during the probe trial (PT) that was conducted after every 4 training trials. Even though the target was displaced after PT6, the actor-critic agent continued to navigate to and circle around the PT6 target location while struggling to relearn new policies for the displaced targets in PT7, PT8 and PT9. The symbolic and the neural agents

demonstrate successful few-shot navigation from about PT4 as their trajectories end up in the region of the displaced target locations after 4 training trials.

### Faster navigation past an obstacle to single goal by hybrid agents

Having shown that symbolic and neural agents both perform one-shot learning of single displaced goals, we further studied their ability to navigate to a single goal with an obstacle in the arena. The goal (shown as a red dot) and obstacle (shown as black circles) were placed as shown in the right of Figure 4A, as well as in Figure 4C. During each trial, agents started from the north, east, or west midpoints of the arena. Starting from the south midpoint was excluded, so that a direct path to the goal was impossible. Training was organized over 60 trials with 18 unrewarded probe trials during trials 7-12, 30-36 and 54-60.

Besides the actor-critic, symbolic, and neural schema agents (Fig. 3A), two hybrid actor-critic-schema agents were developed. The actor-critic-symbolic agent used the symbolic implementation (Fig. 4A, left) while the actor-critic-neural agent used the fully neural implementation (Fig. 4A, right) of LEARN FLAVOR-LOCATION and NAVIGATE. The actor received inputs from both the reservoir and NAVIGATE (Eq. 9). Relative contributions from each were parameterized by  $\beta^{control}$ , where  $\beta^{control} = 0.3$  for the hybrid actor-critic schema agents means input to the actor was 30% from NAVIGATE and 70% from the reservoir;  $\beta^{control} = 0$  is a pure actor-critic agent;  $\beta^{control} = 1$  is a pure schema agent.

Figure 4B shows the latency required to reach the goal (left) and the average amount of time spent at the goal during the probe trials (right). The latency of the actor-critic, actor-critic-symbolic, and actor-critic-neural agents decreased significantly from  $182 \pm 9.1$  s in the first trial to  $58 \pm 4.4$  s,  $44 \pm 3.3$  s, and  $52 \pm 3.6$  s, respectively, in the last trial. The time spent at the goal increased from PT1 to PT3 for the actor-critic ( $t = 35.1, p < 10^{-4}$ ), actor-critic-symbolic ( $32.8, p < 10^{-4}$ ), and actor-critic-neural ( $F = 37.0, p < 10^{-4}$ ) agents during the probe trials as learning progressed.

On the other hand, the neural agent's latency decreased only slightly to  $120 \pm 7.8$  s, while the symbolic agent's latency increased to  $222 \pm 8.7$  s. The time spent at the target increased for the neural agent ( $t = 18.6, p < 10^{-4}$ ) while it decreased for the Symbolic agent ( $t = -15.3, p < 10^{-4}$ ). Thus, the pure schema agents did poorly, but the actor-critic and the hybrid actor-critic-schema agents did well navigating past the obstacle.

Figure 4C shows the example trajectories (top) and value and policy maps for all agents during PT3. The actor-critic navigates past the obstacle as it learns actions based on its location in the arena, which was consistent with the results of previous studies (Frémaux et al., 2013).

The symbolic agent initially reached the goal, but performance worsened after PT1. During the initial trials, the schema agent was still learning the metric representation, hence the direct heading specified by NAVIGATE in PT1 was suboptimal (Fig. 4C, yellow trajectory for symbolic  $\beta^{control} = 1$ ). As the metric representation converged, NAVIGATE specified the agent to head directly to the goal in PT3. However, the direct heading policy caused the agent to get stuck at the obstacle (Fig. 4C, green trajectories for symbolic  $\beta^{control} = 1$ ), until the goal coordinate was deleted at the end of the trial when no reward was disbursed.

The neural agent also moved partly by direct heading, but stochasticity in the goal coordinates and reward recall value due to the changing contribution of place cell activity during navigation and decaying goal representation caused enough randomness in the agent's trajectories for it to perform better than the symbolic agent in PT3 (Fig. 4C, green trajectories for neural  $\beta^{control} = 1$ ). The randomness was partly due to NAVIGATE suppressing direct heading when fluctuations in the reward recall value brought it below the threshold (Supplementary Fig. 1B). Nonetheless, the neural agent performed much more poorly than the agents with an actor-critic.

Hybrid actor-critic schema agents were better than the pure actor-critic agent in some ways. The actor-critic and actor-critic-neural agents had comparable latencies (one-way ANOVA  $F = 0.918, p =$

0.341), while the actor-critic-symbolic agent had the shortest latency (one-way ANOVA  $F = 23.3$ ,  $p < 0.001$ ). Both the actor-critic-symbolic (PT1:  $t = 253$ ,  $p < 10^{-4}$ , PT2:  $t = 298$ ,  $p < 10^{-4}$ , PT3:  $t = 187$ ,  $p < 10^{-4}$ ) and actor-critic-neural (PT1:  $t = 47$ ,  $p < 10^{-4}$ , PT2:  $t = 67$ ,  $p < 10^{-4}$ , PT3:  $t = 82$ ,  $p < 10^{-4}$ ) agents spent more time at the goal location during probe trials than the actor-critic agent. The value and policy map for the hybrid agents show a mixed policy, partly contributed by the actor-critic and partly contributed by the schema component. This could facilitate the agents navigating away from the obstacle and then turning towards the goal by direct heading when there is no obstruction to a direct path (Fig. 4C).

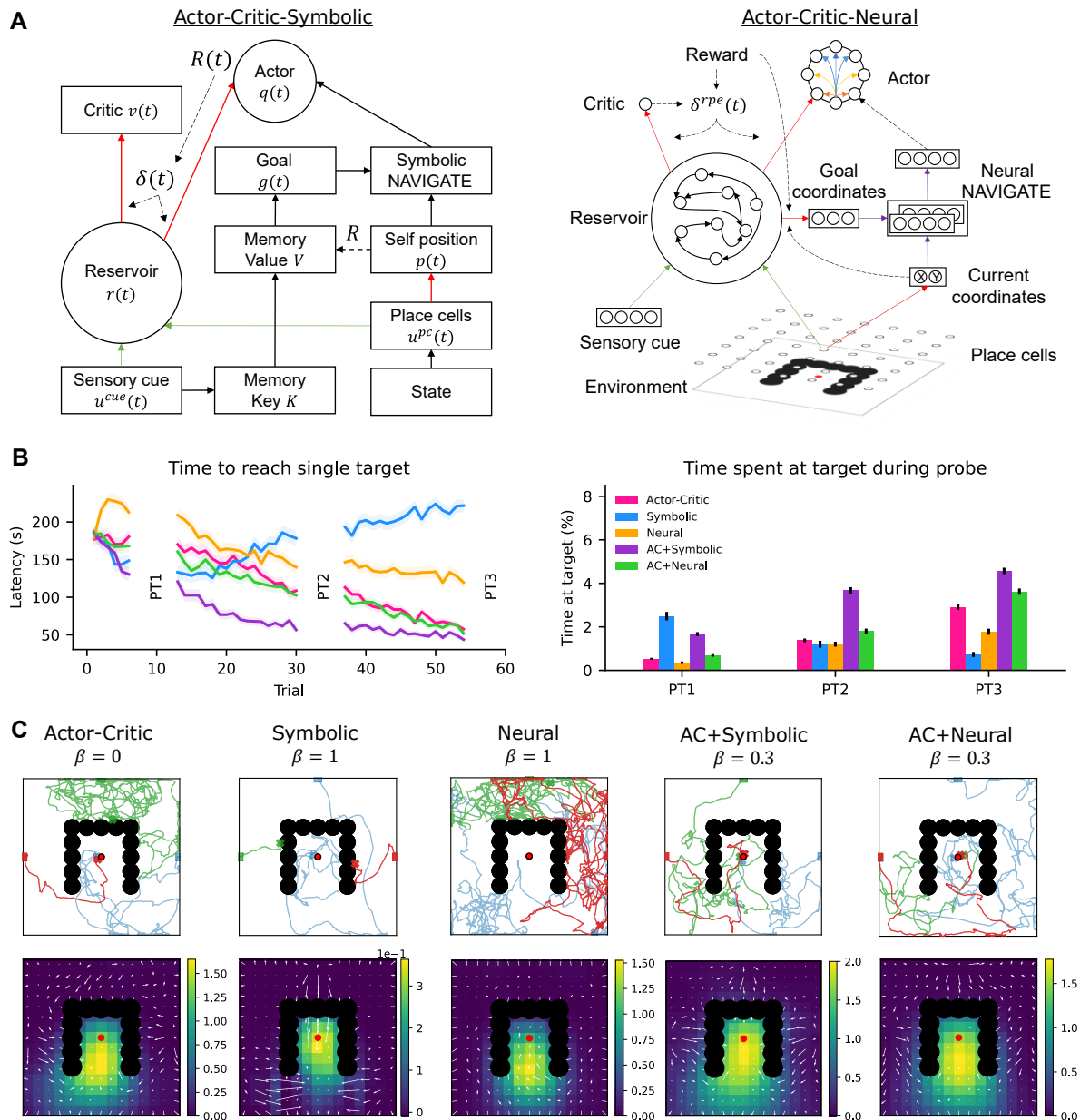


**Figure 4. Navigating past an obstacle to a single goal.** A) Two hybrid actor-critic-schema architectures were developed that combined the actor-critic with either symbolic (left) or neural (right) schemas. B) The actor-critic (pink) and the hybrid actor-critic-schemas (actor-critic-symbolic – purple, actor-critic-neural – green) showed decreasing latency (left) and spent a higher proportion of time at the goal during the probe trials (right), whereas the pure schema agents (the Symbolic (blue) more so than the Neural (orange) agents) struggled to navigate past the obstacle and incurred increasing, or slower, decreases in latencies, respectively. C) Example trajectories (top) during Probe Trials 1 (blue), 2 (green), and 3 (red) show both actor-critic ( $\beta = 0$ ) and actor-critic-schema agents ( $\beta = 0.3$ ) chose actions to navigate past the obstacle and towards the goal, while the pure schema agents ( $\beta = 1$ ) moved only by direct heading and got stuck at the obstacle. The policy (white arrows) and value (colormap) maps

(bottom), respectively, show actor and critic outputs. Hybrid actor-critic schema agents learned policies that had aspects of both pure actor-critic and pure schema policies. 480 simulations were performed for each type of agent, with the shaded area and error bars indicating 95% confidence intervals.

## One-shot learning of multiple paired association navigation

Having shown that both the symbolic and neural schema agents demonstrate one-shot learning of single displaced goals, we now study one-shot learning of multiple flavor-location associations. The task was in 2 stages. The first stage requires learning six flavor-location associations over 20 sessions; the second stage requires learning two or six new paired associations in a familiar or novel environment for one session.

The first stage was organized into 20 sessions, each consisting of six trials across which the agent was exposed to Flavor Cues 1–6 in random order. Each cue was presented throughout the trial, and the agent received a reward only if it reached the corresponding goal (insets in Fig. 5A (right) and Fig. 5B (left) show reward locations). Training was interspersed with three non-rewarded probe sessions during Session 2 (PS1), Session 9 (PS2), and Session 16 (PS3).

The second stage consisted of one session with the original paired associations (OPA), two new paired associations (2NPA), six new paired associations (6NPA), or a new maze (NM) condition. A non-rewarded probe session followed for each condition.

Tse and colleagues (2007) demonstrated one-shot learning in the 2NPA condition, which introduces two new flavor-location associations with Cues 7 and 8 replacing Cues 1 and 6, while cue–locations 2–5 remained. We also explore a more difficult version of that problem, the 6NPA condition, which introduces six new associations with cues 1–6 replaced by cues 11–16.

Tse and colleagues (2007) demonstrated abolishment of one-shot learning in the NM condition, which had the same flavor-location associations as 6NPA, but the environmental cues around the arena were different from the first stage (the environmental cues remained the same as in the first stage for all other second stage conditions). We postulated that the new environmental cues caused place cell remapping, which invalidated the metric representation learned in the first stage, and prevented one-shot learning in the second stage. To model place cell remapping, place cell selectivity was shuffled at the start of NM so that each place cell was anchored to a different location.

In the first stage, all agents gradually learned all six flavor-location pairs. The latency required to reach all six goals gradually decreased to  $25 \pm 1.6$  s,  $46 \pm 2.6$  s, and  $67 \pm 2.9$  s for the actor-critic, symbolic, and neural schema agents, respectively, by Session 20 (Fig. 5A, left). During the non-rewarded probe sessions, the visit ratio was calculated as the amount of time spent within 0.1 m from the centre of the correct goal divided by the time spent within 0.1 m of any of the six possible goals; a visit ratio of 16.7% was consistent with chance performance, where the agent visited all six reward locations equally or visited one location regardless of cue. All agents showed improvements in visit ratios from PS1 to PS3 (Fig. 5B, right), with the Symbolic and Neural agents achieving above chance visit ratios in all probe sessions (t-tests after subtracting chance performance of 16.7%,  $t > 27$ ,  $p < 10^{-4}$ ) while the actor-critic which showed chance performance for PS1 ( $t = -4.8$ ,  $p = 1.0$ ) and above chance performance for PS2 ( $t = 53$ ,  $p < 10^{-4}$ ) and PS3 ( $t = 105$ ,  $p < 10^{-4}$ ).

In the second stage, the symbolic and neural schema agents demonstrated one-shot learning of two or six new paired associations (Fig. 5B), as shown by above chance visit ratios for the two new locations in 2NPA (symbolic:  $t = 108$ ,  $p < 10^{-4}$ , neural:  $t = 71$ ,  $p < 10^{-4}$ ) and the six new locations in 6NPA (symbolic:  $t = 679$ ,  $p < 10^{-4}$ , neural:  $t = 140$ ,  $p < 10^{-4}$ ). The actor-critic agent did not show one-shot learning, with chance visit ratios for both 2NPA ( $t = -19$ ,  $p = 1.0$ ) and 6NPA ( $t = -5.9$ ,  $p = 1.0$ ) conditions. All agents performed well in the OPA condition in which one-shot learning was not required, as the paired associates were the same as in the first stage. However, none of the agents displayed one-shot learning in the NM condition. Example trajectories for the agents during the first stage (PS1, P2, PS3) and the various second stage conditions (OPA, 2NPA, 6NPA, NM) are shown in Figure 5D.

All agents had distinct policy and value maps for each of the six paired associates in the OPA condition (example maps shown for Cue 2 in Fig. 5E) where the peak in the value map corresponds to the cue specific location and the policy map demonstrates the path to reach the correct target.

However, only the schema agents demonstrated cue-specific value and policy maps for each of the new paired associates after one session in the 2NPA or 6NPA conditions. The actor-critic maps for different cues were not sufficiently distinct, contributing to the chance performance (example maps for Cue 7 and Cue 16 shown in Fig. 5E).

In the NM condition, all agents performed poorly after one session with chance-level visit ratios (Fig. 5B). The schema agents were unable to estimate their coordinates accurately (Supplementary Fig. 3), causing them to meander around the arena while the actor-critic resorted to explorative trajectories (Fig. 5D). To determine if continued NM training would enable agents to learn a metric representation that enables one-shot learning, the agents continued for a total of 20 sessions with Cues 11–16. This was followed by a third stage in which we introduced six new flavor-location pairs (6NPANM) with Cues 7–10, 17, and 18 for a single session, followed by a non-rewarded probe session (Supplementary Fig. 4). Over the 20 sessions, both the actor-critic and schema agents demonstrated gradual learning of the six paired associates (Supplementary Fig. 4A). More importantly, when the agents were introduced to six new paired associations in the new maze condition, the schema agents demonstrated one-shot learning of 6NPANM, while the Actor-Critic failed to do so (Supplementary Fig. 4B, C).

To study the agents' one-shot learning capacity, 12 new paired associates were introduced for a single trial each after learning the OPA configuration over 20 sessions (Fig. 5C). For each agent simulation, the goal locations for the 12 paired associates were randomly chosen out of the 43 remaining reward locations, after excluding the six reward locations that were used for the OPA condition. We arbitrarily defined a paired associate to have been learned if an agent achieved a visit ratio of more than 16.7% for the pair, well above the 8.3% expected if all 12 goals were visited randomly (see Supplementary Fig. 4D for example trajectories for 12NPA). The actor-critic learned  $1.9 \pm 0.17$  paired associates; the symbolic agent learned  $11.58 \pm 0.12$  paired associates after just one session of learning; neural agents either with a nonlinear feedforward layer or reservoir trained using the LMS or EH rules demonstrated a monotonic increase in one-shot learning performance when the number of hidden or recurrent units were increased from 128 to 2048. For example, the agent with a reservoir of 128 units trained with the EH rule learned  $3.5 \pm 0.11$  paired associates after one trial but the one-shot learning capacity increased monotonically to  $7.8 \pm 0.16$  paired associates when the size of the reservoir was increased to 1024. Interestingly, the agent with a reservoir demonstrated higher one-shot learning capacity compared to the agent with a feedforward layer. Although the LMS rule affords better one-shot learning performance compared to the EH rule, the latter has been argued to be more biological due to the sparseness of the global modulatory factor and the involvement of both presynaptic and postsynaptic terms (Hoerzer et al., 2012). When the agent with a reservoir of 2048 units was trained using the EH rule, the one-shot learning capacity surprisingly decreased to  $3.9 \pm 0.17$  paired associates (as shown in Fig. 5C) but increased to  $8.7 \pm 0.18$  paired associates when the learning rate  $\eta_{goal}$  was reduced from  $7.5 \times 10^{-5}$  to  $5 \times 10^{-5}$ .

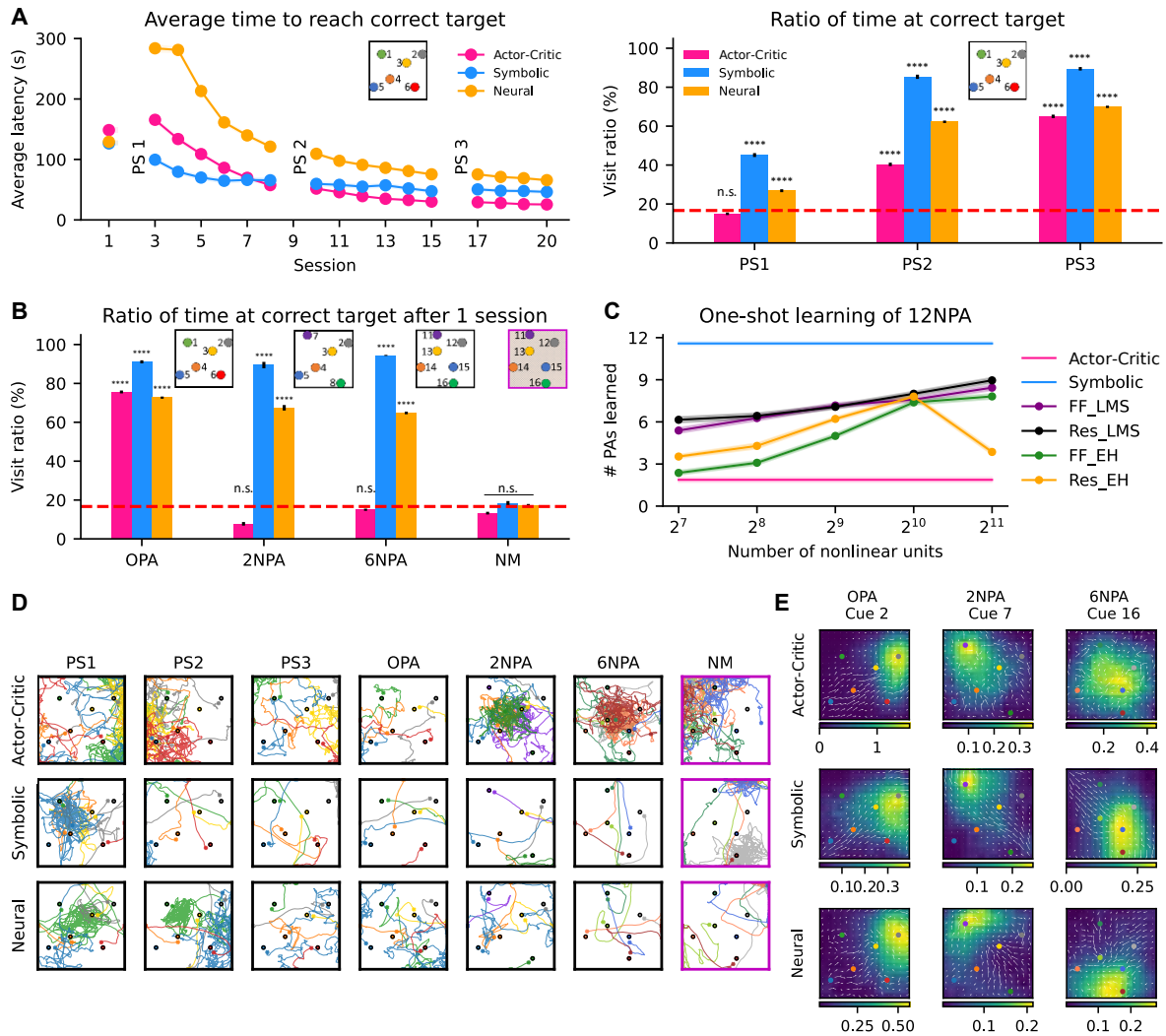


**Figure 5. Gradual one-shot learning of multiple new paired associations.** The task was trained in 2 stages. The first stage consisted of 20 sessions, each with of six trials across which the agent was exposed to six cues, and the agent received a reward only if it reached the corresponding goal. Training was interspersed with three non-rewarded probe sessions during Session 2 (PS1), Session 9 (PS2), and Session 16 (PS3). The second stage consisted of one session with the original paired associations (OPA), two new paired associations (2NPA), six new paired associations (6NPA), or a new maze (NM) condition. A non-rewarded probe session followed each condition. A) In the first stage, the actor-critic (pink), symbolic (blue), and neural (orange) agents demonstrated a gradual decrease in the average latency to reach six cue-specific goals and spent an increasing ratio of time at the correct target across probe sessions PS1, PS2, and PS3. B) In the second stage, all agents showed above chance visit ratios for the OPA condition. Only the symbolic and neural agents showed above chance visit ratios during the 2NPA and 6NPA conditions, demonstrating one-shot learning of two and six new paired associates. All agents demonstrated chance performance after one session in the NM condition. Chance performance was 16.7% (one out of six targets visited). C) After 20 sessions of training in the OPA condition, agents were introduced to 12 new paired associates for a single trial with reward locations randomly chosen out of 43 positions. The actor-critic agent learned at most one paired associate while the symbolic agent learned all 12 paired associates. Neural agents with a feedforward layer or reservoir trained with the LMS or EH rule showed a monotonic increase in one-shot learning capacity when reservoir size was increased from 128 to 1024 units. The reservoir-based schema agent learned more paired associates than the feedforward-based agent with the same number of nonlinear units. D) Example trajectories during PS1, PS2, PS3, OPA, 2NPA, 6NPA, and NM. Trajectory colors correspond to the cue-specific targets. E) The actor-critic agent could not learn distinct value and policy maps after a single trial for cue 7 and 11 while both symbolic and neural agents learned cue specific maps after a single trial of learning. 720 simulations were performed per agent, shaded area and error bars indicate 95% confidence interval. Asterisks \*\*\*\* indicates t-test against chance performance with  $p$ -value  $< 10^{-4}$ .

## One-shot learning of multiple paired association navigation with an obstacle

We have shown that the schema agents perform one-shot learning of multiple paired association navigation, while the actor-critic agent is unable to. We have also demonstrated that schema agents are unable to navigate past an obstacle to a single goal, while actor-critic agents and the hybrid actor-critic-schema agents can.

Here we study one-shot learning of navigating past an obstacle to multiple goals. The flavor-location configurations for OPA, 2NPA, and 6NPA are as in Figure 5. The arena now has an obstacle that resembles an “H” (Fig. 6C, D). The first stage of the task was extended to 50 sessions with non-rewarded probes during Session 2, 18, and 36. After 50 sessions, agents were introduced to OPA, 2NPA, or 6NPA conditions for a single session followed by a probe session. The agent’s starting position was constrained based on the goal location (see Table 2 in Methods) so that direct heading could not be used to reach the goal.

In the first stage, most agents gradually learned to navigate past the obstacle to reach the correct goal. The latency for all agents, except the symbolic agent, gradually decreased by Session 50 (actor-critic:  $117 \pm 5$  s, symbolic:  $343 \pm 9$  s, neural:  $91 \pm 3$  s, actor-critic-symbolic:  $141 \pm 7$  s, actor-critic-neural:  $79 \pm 4$  s), and the visit ratios increased to above chance performance from PS1 to PS2 to PS3 (Fig. 6A). In the second stage, only the hybrid actor-critic-schema agents demonstrated one shot learning, with above chance visit ratios for the 2NPA (actor-critic-symbolic:  $t = 28$ ,  $p < 10^{-4}$ , actor-critic-neural:  $t = 9.6$ ,  $p < 10^{-4}$ ) and 6NPA (actor-critic-symbolic:  $t = 33$ ,  $p < 10^{-4}$ , actor-critic-neural:  $t = 13$ ,  $p < 10^{-4}$ ) conditions; neither the actor-critic nor the pure schema agents demonstrated one-shot learning, with chance level visit ratios (Fig. 6B). For the actor-critic agent, this might have been because it learned distinct value and policy maps for each cue, allowing it to navigate past the obstacle in the first stage (top left in Fig. 6C, D, and Supplementary Fig. 2). However, it failed to learn to navigate past the obstacle to the new paired associates after a single trial in the second stage. For the symbolic agent, it successfully moved towards the goal using direct heading, but got stuck at the obstacle. Interestingly, the neural agent did not get stuck at the obstacle in the first stage. As in the single goal task with obstacle, the neural agent moved by partly direct heading, but stochasticity in the goal coordinates and reward recall value due to the changing contribution of place cell activity during navigation and decaying goal representation caused enough randomness in the agent’s trajectories to enable it to get past the obstacle. Although this degree of randomness allowed the neural agent to solve the first stage, it failed at one-shot learning in the second stage. The hybrid actor-critic-schema agents overcame the limitations of the actor-critic and pure schema agents by gradually learning a mixed policy to navigate away from the obstacle while using NAVIGATE to head directly to the goals when possible (Fig. 6C, D). This demonstrates that a combination of actor-critic and schema algorithms enables one-shot learning of multiple paired association navigation with an obstacle.

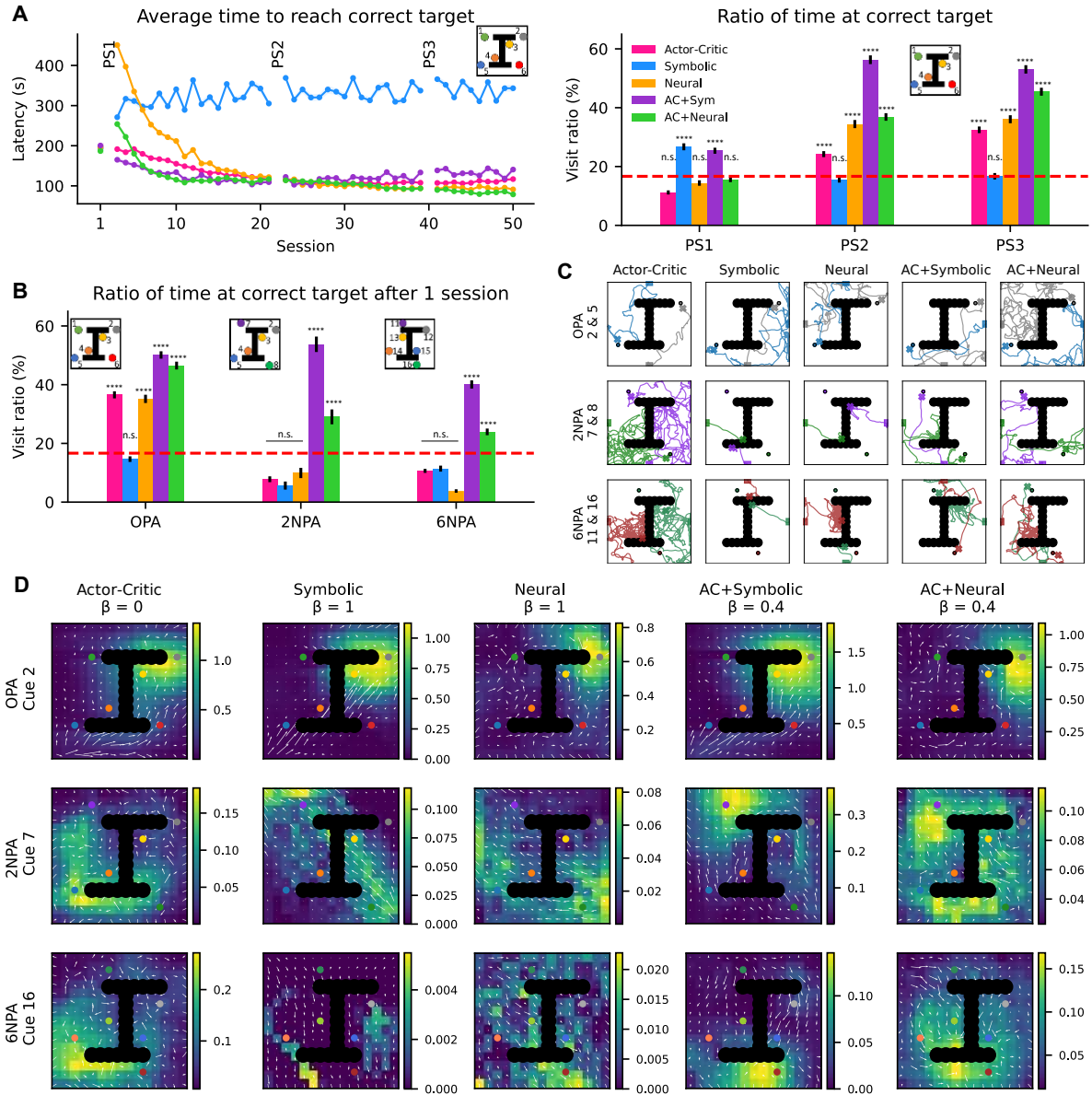


**Figure 6. One-shot learning of multiple paired association navigation with an obstacle by hybrid actor-critic-schema agents.** A) In the first stage, all agents, except the symbolic agent, showed a decrease in average latency for the six paired associates (left) and improvements in visit ratio during the probe sessions (right). B) In the second stage, both the actor-critic-symbolic and actor-critic-neural agents demonstrated one-shot learning in the 2NPA and 6NPA conditions ( $p < 10^{-4}$ ) while the actor-critic, symbolic and neural agents showed chance or below-chance performance of 16.7%. C) Example trajectories for two paired associates by each agent (left to right: actor-critic, symbolic, neural, actor-critic-symbolic, actor-critic-neural) during the OPA (Cue 1 and Cue 6), 2NPA (Cue 7 and Cue 8), and 6NPA (Cue 11 and Cue 16) probe sessions after a single session in the second stage. Although the actor-critic agent can navigate past the obstacle, it cannot navigate to the new goals after a single trial; the pure schema agents cannot navigate past the obstacle after a single trial; only the hybrid agents use a combination of direct heading and state-based actions to navigate past the obstacle and learn new paired associates after a single trial. D) Superimposed value and policy maps of all agents during non-rewarded probe sessions (averaged over 96 simulations per agent). Refer to the insets in Fig. 6B for cue-specific target locations. Only the hybrid agents show appropriate value and policy maps for the new paired associates. 480 simulations were performed per agent, shaded area and error bars indicate 95% confidence interval. Asterisk \*\*\*\* indicates t-test against chance performance with  $p$ -value  $< 10^{-4}$ .

## One-shot learning with working memory and learning to gate working memory

In the previous sections, sensory cues were presented throughout the trial for all tasks. In this section, we used the same two-stage task as in Figure 5 but with the cue presented only at the start of the trial for 2 seconds, as was the case in the biological experiment (Tse et al., 2007). We studied only the hybrid actor-critic-neural agent with  $\beta^{control} = 0.9$  in this section.

We previously showed that a bump attractor can give an actor-critic agent the working memory needed for the first stage of the MPA task with transient cue presentations (Kumar et al., 2022). We therefore explored whether adding a bump attractor could give the actor-critic-neural agent one-shot learning ability in the MPA task when cues were transiently presented. We added a bump attractor that took in the sensory cues as inputs with weights such that each cue activated a different subpopulation within the bump attractor and attractor dynamics persistently maintained cue information throughout the trial. The bump attractor activity was passed to the reservoir as an additional input (Fig. 7A).

To study a version of the task with distractors, Cue 17 or 18 was randomly chosen as the distractor and presented 3 seconds after the task relevant cue, at a mean rate of 0.2 Hz for a duration of one second. Each distractor caused a different subpopulation of the bump attractor to be excited. A distractor was presented either once or twice within a trial to increase the probability of disrupting the cue information maintained by the bump attractor. When a cue is transiently presented, the bump attractor's persistent activity maintains a representation of the cue. However, distractor presentation causes the bump attractor to update the working memory with distractor information (Fig. 7B).

As such, the bump attractor alone is not able to ignore the distractors. We therefore added a working memory gating mechanism that allows or restricts the flow of information from the sensory cue to the bump attractor (Lloyd et al., 2012; O'Reilly & Frank, 2006; Todd et al., 2009). The gating mechanism consists of the reservoir sending input to two gating units, only one of which is active at a time due to a winner-take-all rule; one of the gating units multiplicatively modulates information flow from the cue to the bump attractor, such that the information flow is permitted only when that gating unit is active. The TD error used in the actor-critic can also be used in a learning rule governing the synaptic weights from the reservoir to the gating units (Eq. 45). The winner-take-all rule and the multiplicative modulation are not neurally implemented in our simulations, but the learning rule for the synapses from the reservoir to the gating units is biologically plausible.

The first stage of the task was set to 20 sessions with non-rewarded probes during Sessions 2, 9, and 16. After 20 sessions, agents were introduced to OPA, 2NPA, or 6NPA conditions for a single session followed by a probe session. The TD error (purple) and the gating activity (green,  $\chi(t)$ ) were averaged across all six cues in each probe session (Fig. 7C). After one training session (PS1), the TD error spiked at cue presentation (red bars) and was sharply depressed when the cue was silenced, then returned and remained close to zero during distractor presentation (blue bars); the gating activity remained near 0.45, meaning there was almost equal probability of updating or maintaining working memory. After six additional training sessions (PS2), the TD error continued to spike at the onset of the cue but also spiked when the cue was silenced; more importantly, the gating activity was near 0.5 during cue presentation but quickly dropped to about 0.11 when the cue was silenced. The pattern of TD error and gating activity in PS2 remained not only in PS3 and the OPA condition, which had the same set of paired associates, but also in the 2NPA and 6NPA conditions, which had new paired associates. This suggested that learning to gate working memory does not need to be relearned when there are new cues.

When distractors were absent and synaptic plasticity for the gating mechanism was switched off (green), the agent succeeded in the first stage of the task (Fig. 7D) and the OPA condition in the second stage (Fig. 7E) without learning to gate working memory. The agent's average latency to 6 paired associates (Fig. 7D, top) gradually decreased from  $143 \pm 5$  s in Session 1 to  $56 \pm 3$  s in Session 20 and the visit ratio improved (Fig. 7D, bottom) from PS1 to PS3 ( $t = 85.4, p < 10^{-4}$ ) and OPA ( $t = 100, p < 10^{-4}$ ). When there were one (light blue) or two distractors (dark blue), the latency only decreased to  $133 \pm 6$  s and  $178 \pm 7$  s in Session 20 respectively, and visit ratios during PS1, PS2, PS3, and OPA were lower than when there were no distractors (with one distractor:  $F = 654, p < 10^{-4}$ , with two

distractors:  $F = 277, p < 10^{-4}$ ). When the synaptic plasticity was switched on, performance with distractors gradually improved. Agents achieved a greater decrease in latency to  $71 \pm 4$  s and  $87 \pm 5$  s for one (yellow) and two (red) distractors, respectively, and higher visit ratios during probe sessions PS1 to PS3 and OPA (with one distractor:  $F = 2486, p < 10^{-4}$ , with two distractors:  $F = 1670, p < 10^{-4}$ ) compared to when synaptic plasticity was switched off.

In the second stage of the task, one-shot learning of new paired associates with a transiently presented cue was possible without learning to gate working memory; this was seen in the above chance visit ratios in the 2NPA and 6NPA conditions when synaptic plasticity for the gating mechanism was switched off (green bars in Fig. 7E); this showed that adding a bump attractor was sufficient for one-shot learning that reproduced the observed rodent behavior. However, visit ratios for 2NPA decreased to chance (one distractor:  $t = 1.6, p = 0.0571$ , two distractors:  $t = 1.2, p = 0.115$ ) and visit ratios for 6NPA (one distractor:  $t = -8.6, p < 10^{-4}$ , two distractors:  $t = -23.8, p < 10^{-4}$ ) were significantly lower compared to when no distractors were presented (light blue and dark blue bars in Fig. 7E), demonstrating that the bump attractor without learning to gate working memory was insufficient for one-shot learning when distractors were present. However, when synaptic plasticity for the gating mechanism was switched on, the transfer of the working memory gating learned by PS2 to the 2NPA and 6NPA conditions (Fig. 7D) allowed the agent to show one-shot learning when distractors were present; visit ratios for 2NPA (one distractor:  $t = 9.8, p < 10^{-4}$ , two distractors:  $t = 17, p < 10^{-4}$ ) and 6NPA (one distractor:  $t = 32, p < 0.001$ , two distractors:  $t = 40, p < 10^{-4}$ ) were higher compared to when the synaptic plasticity was switched off (yellow and red bars in Fig. 7E).

Finally, we report synaptic weight changes (Fig. 7F), as these have been used to compare model predictions with biological observations (McClelland, 2013; Tse et al., 2011). Synaptic weight change was the average squared difference between the synaptic weights before and after an OPA, 2NPA, 6NPA, or NM session in the second stage. The weight change for synapses onto the goal neurons increased from OPA to 2NPA to 6NPA, but was higher for 2NPA (t-test  $t = 3.9, p < 0.001$ ) and 6NPA (t-test  $t = 13, p < 10^{-4}$ ) compared to NM, and was thus nonmonotonic overall with the increasing novelty from OPA to 2NPA to 6NPA to NM; the lower rate of finding goals in NM likely lowered the amount of goal synapse plasticity. The weight change for the synapses onto the coordinate neurons (ANOVA  $F = 9658, p < 10^{-4}$ ) and the gating units (ANOVA  $F = 33, p < 10^{-4}$ ) generally increased with increasing novelty from OPA to NM, even though 2NPA and 6NPA produced comparable weight changes for the coordinate neurons (t-test  $t = 1.2, p = 0.237$ ). The actor and critic patterns differed from those of the goal neurons, coordinate neurons, or gating units; the weight change for synapses onto the actor and the critic was lowest in the OPA condition; the weight change of the synapses onto the actor in 2NPA was comparable to that in NM (t-test  $t = 0.5, p = 0.619$ ), and higher in 6NPA than in NM (t-test  $t = -2.2, p < 0.05$ ), while the weight change of the synapses onto the critic was comparable between 2NPA and NM (t-test  $t = 1.6, p = 0.113$ ), as well as between 6NPA and NM (t-test  $t = -0.96, p = 0.338$ ).

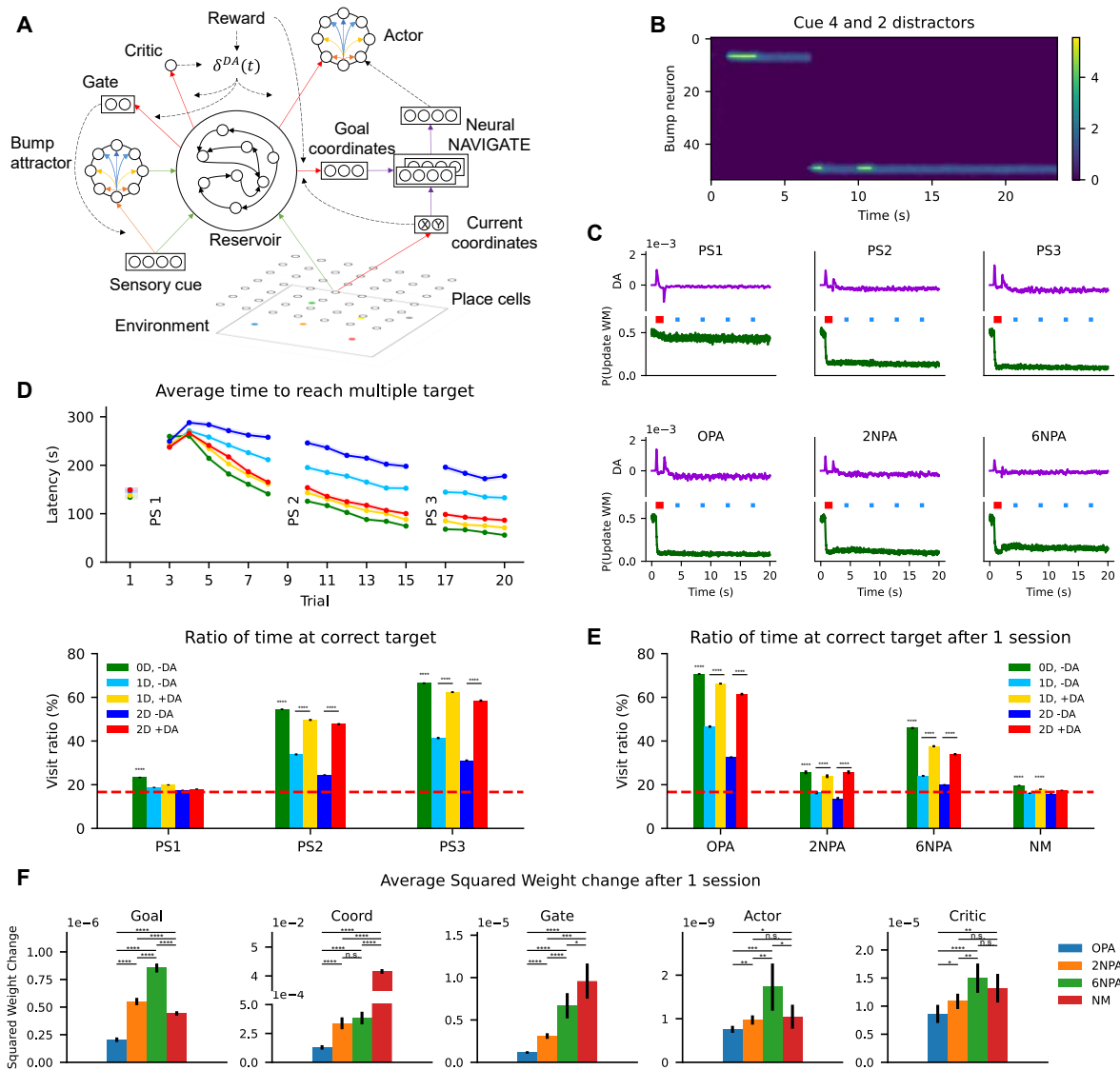


**Figure 7. Learning to gate working memory generalizes to new paired associates.** A) A bump attractor and working memory gating mechanism was added to the actor-critic-neural agent. The synapses from the reservoir to the gating units were modified using a form of TD error-modulated plasticity. B) The bump attractor maintains a persistent representation of a transient cue, but presentation of a distractor updates the working memory with distractor information. When Cue 4 was presented, a subpopulation of bump attractor neurons selective for Cue 4 were persistently activated until distractor Cues 17 and 18 were presented to activate different subpopulations. C) The TD error (purple) and gating activity (green) averaged across all six cues in each probe session are shown for PS1, PS2, PS3, OPA, 2NPA, and 6 NPA conditions with plasticity of the synapses onto the gating units switched on. The policy gradually learned through PS1 and PS2 was maintained for PS3 and OPA in which the paired associates remained the same, and transferred to 2NPA and 6NPA even though these included new paired associates that had been only encountered in a single trial. D) Latencies (top) and visit ratios (bottom) for agents with plasticity of the synapses to the gating units switched off (-DA) or on (+DA) with zero (0D), one (1D), or two (2D) distractors; different colors indicate different conditions; each color indicates the same condition for bottom and top panels. In the first stage of the task, as the number of distractors increased from zero (green) to one (light blue) to two (dark blue) when plasticity was switched off, agents took a longer time to reach the goal (top) and spent less time at the goal (bottom); as the number of distractors increased from zero (green) to one (yellow) to two (red) when plasticity was switched on, agents were more comparable in the time needed to reach the goal (top) and the time spent at the goal (bottom). E) Agents one-shot learning ability when distractors were present was rescued when synaptic plasticity for the gating mechanism was switched on. F) Synaptic weight change as novelty increases from OPA to 2NPA to 6NPA to NM for synapses onto the goal neurons, coordinate neurons, gating units, actor, and critic. 480 simulations were performed per agent, shaded area and error bars indicate 95% confidence intervals. Asterisks indicates t-test against chance performance and a line underneath the

asterisks indicates a paired t-test.

## Discussion

Tse and colleagues developed a rodent multiple paired association navigation task for studying schemas in one-shot learning (Tse et al., 2007), but conceptualization of the schemas, their role in enabling one-shot learning, and their biologically plausible implementation remained unclear. We have therefore described schemas that could underlie the observed rodent behavior in conceptual terms roughly corresponding to Marr's Computational Level (Marr, 2010; Marr & Poggio, 1977; Poggio, 2012), outlined symbolic or machine learning algorithms that could perform the computations, explained how each schema has a counterpart biologically plausible implementation, and composed these schemas into a fully neural network-based agent in which synaptic plasticity is governed by biologically-plausible rules, and that replicates rodent one-shot learning in the multiple paired association navigation task.

We built on the one-shot learning agent of Foster and colleagues, which was based on biologically plausible synaptic plasticity and can be thought of as composed of 3 schemas: LEARN METRIC REPRESENTATION, LEARN GOAL COORDINATES, and NAVIGATE; however, their LEARN GOAL COORDINATE and NAVIGATE schemas were symbolic, and one-shot learning was for single goals (Foster et al., 2000). We refined LEARN METRIC REPRESENTATION and trained a neural network that approximates the symbolic computation performed by NAVIGATE schema. More importantly, we replaced LEARN GOAL COORDINATES with LEARN FLAVOR LOCATION in which a feedforward layer or reservoir with readout units is trained by the reward-modulated EH rule to associate each of multiple cues with their goal coordinates after one trial.

Hopfield networks are canonical Hebbian plasticity-based models that are capable of one-trial association, and have been conjectured to describe the highly recurrent hippocampal CA3 region (Hopfield, 1982; Krotov & Hopfield, 2021; Pfeiffer & Foster, 2015; Rolls, 2007, 2013; Whittington et al., 2020). However, Hopfield networks suffer from at least two problems. The first problem is difficulty with continual learning, because once a set of patterns are stored, additional patterns cannot be stored without disrupting previous associations (Fusi, 2021; Parisi et al., 2019). Techniques such as pseudo-rehearsals are needed to store new patterns simultaneously with the old patterns (Frean & Robins, 1999; Robins, 2004). Although activity replay (Carr et al., 2011; Ji & Wilson, 2007; Karlsson & Frank, 2009) could be a biological mechanism for pseudo-rehearsals, that requires additional neural circuitry to store and recall memories (Nicola & Clopath, 2019; van de Ven et al., 2020). The second problem is that if we wish, for example, to associate the cue vector and the goal coordinates, that activity may need to be transformed into a representation suitable for association, then inverse transformed to retrieve the goal coordinates; the transformations may be obtained by training neural networks using backpropagation (Banino et al., 2018; Limbacher & Legenstein, 2020; Whittington et al., 2020). Our neural implementation of LEARN FLAVOR-LOCATION appears not to suffer from the continual learning problem in the regime we examined, and outputs the goal coordinates for each cue.

We previously showed that a non-schema-based, model-free reinforcement learning actor-critic with biologically-plausible synaptic plasticity learns to navigate past an obstacle to multiple paired associates in the first stage of the MPA task (Kumar et al., 2022). Consistent with Tse and colleagues' proposal that the task sheds light on schemas for one-shot learning (Tse et al., 2007), the actor-critic fails at one-shot learning in the second stage. Nonetheless, an actor-critic can improve schema-based agents, as the hybrid actor-critic-schema agents succeeded at one-shot learning in the two-stage MPA task with an obstacle, even though the schema-based agents performed poorly when an obstacle is present.

The plasticity rules in LEARN METRIC REPRESENTATION and LEARN FLAVOR-LOCATION are biologically plausible in that plasticity at a synapse depends on local factors (such as the presynaptic and postsynaptic activities) and global neuromodulatory factors, but not on non-local synapse-specific factors. Learning a metric representation requires an error term to be computed for each coordinate axis and presynaptic activity in the form of an eligibility trace encapsulating place cell activity. This takes

the form of a non-Hebbian two-factor learning rule in which plasticity depends on presynaptic activity and a global modulatory factor, but not postsynaptic activity; this resembles learning rules in hippocampal CA3 (Castillo, 2012; Castillo et al., 1994; Katsuki et al., 1991; Langdon et al., 1995; Nicoll & Schmitz, 2005; Urban & Barrionuevo, 1996; Zalutsky & Nicoll, 1990), the cerebellum (Hausknecht et al., 2017; Medina & Mauk, 1999; Piochon et al., 2013), and the amygdala (Humeau et al., 2003). Prior work suggests that three-factor modulated Hebbian plasticity, which depends on postsynaptic activity, may succeed like the two-factor rule (Frémaux et al., 2013). Plasticity at the goal synapses requires all three factors, and an additional reward modulation factor; our proposal of a 4-factor rule was inspired by 3-factor modulated Hebbian plasticity (Frémaux & Gerstner, 2016; Hoerzer et al., 2012).

The key to our model of gradual then one-shot learning in the two-stage MPA task is that there are at least two learning processes: a slow process and a fast, one-shot process. Learning is initially gradual as it involves both processes, but then becomes one-shot once the slow process has completed, and new learning depends only on the fast process. Fundamentally, a successful model does not seem to require that the slow learning process be associated with a schema. However, our simulations include two slow learning processes, each of which can be associated with a schema or structure beyond the simplest actor-critic agent. In our main agent (Fig. 5), the neural implementation of the LEARN METRIC REPRESENTATION schema is the slow learning process. In the agent with working memory (Fig. 7), learning to gate working memory is another slow learning process; while we do not provide a computational level description of the process as a schema, learning to gate working memory involves more structure than the simplest actor-critic agent, even though it minimizes the same TD error. Whether a sharp distinction between learning with a schema and the simplest model-free actor-critic remains to be clarified, possibly analogous to the question of a sharp distinction between model-based and model-free reinforcement learning (Dolan & Dayan, 2013).

Unlike the main agent, the agent that learned to gate working memory did not receive a fully neural implementation; its learning rule for the synapses from the reservoir to the gating units was biologically plausible, but its winner-take-all rule and multiplicative modulation were not neurally implemented; perhaps a fully neural implementation can be developed (Frémaux et al., 2013). Although we did not do so here, our main point was to show that relevant slow learning processes may include possibilities other than LEARN METRIC REPRESENTATION.

Interestingly, the slow learning processes of LEARN METRIC REPRESENTATION and learning to gate working memory exhibited monotonic synaptic weight changes with the increasing novelty from OPA to 2NPA to 6NPA to NM (Fig. 7G), resembling gene expression changes in the hippocampus (Tse et al., 2011); while the fast, one-shot learning process of LEARN FLAVOR-LOCATION exhibited a nonmonotonic weight change (Fig. 7G), resembling gene expression changes in the prefrontal cortex (Tse et al., 2011); the nonmonotonic weight change of LEARN FLAVOR-LOCATION may reflect less success in finding the target with one-shot acquisition in NM than in the 2NPA and 6NPA conditions, and may reflect the dependence of one-shot learning on appropriate slow learning having already taken place (Gilboa & Marlatte, 2017; McClelland, 2013; Tse et al., 2011).

Computational models have used vector-based navigation or direct heading for one-shot navigation (Banino et al., 2018; Howard et al., 2014; Ito et al., 2015; Lyu et al., 2022). Behavioral evidence suggests animals perform vector-based navigation (Etienne et al., 1998; Müller & Wehner, 1988). Hence, NAVIGATE performs vector subtraction between the animal's current location and goal to compute the direction and distance for direct heading. There are several proposals for how the brain computes the vector subtraction (Bicanski & Burgess, 2020; Nyberg et al., 2022; Poucet & Hok, 2017), some of which involve direct decoding of position into an explicit metric representation, as performed here by the coordinates learned by LEARN METRIC REPRESENTATION (Bush et al., 2015; Fiete et al., 2008; Foster et al., 2000). Hippocampal subiculum neurons whose activity resembles the encoding

of Cartesian coordinates by the coordinate neurons in our models have been described, for example, in Figures 2B, 2D, 2F of Lever et al. (2009); postrhinal cortex neurons whose activity represent polar coordinates have been described, for example, in Figures 1C, 1E, 1G of LaChance et al. (2019). There are several possibilities for how the direction and distance for direct heading are represented in the hippocampus (Høydal et al., 2019; Ormond & O’Keefe, 2022; Sarel et al., 2017; Spiers et al., 2018), including neurons in Fig. 3D, 3F of Sarel et al. (2017) whose activity is inversely related to the activity of the actor neuron that signals the preferred action in our model.

A limitation of our agents is that NAVIGATE only affords direct heading. Although combining NAVIGATE with an actor-critic allowed agents to use trial and error to navigate past an obstacle, incorporation of model-based methods such as options (Botvinick, 2012), subgoals (McGovern & Barto, 2001), successor representations (Dayan, 1993; Gardner et al., 2018; Stachenfeld et al., 2017) or path planning algorithms (Stentz, 1997) would perhaps allow agents to plan trajectories around obstacles (Daw et al., 2011; Gläscher et al., 2010).

Gene expression and neural inactivation experiments suggest that the hippocampus and prefrontal cortex are important for the gradual then one-shot learning in the two-stage MPA task (Tse et al., 2011). As discussed above, many elements of our computational agents have potential counterparts in the hippocampus, prefrontal cortex, and associated regions. Additionally, the actor-critic may be associated with the basal ganglia (Kumar et al., 2022), while working memory and its gating may involve the prefrontal cortex, basal ganglia, and thalamus (Mukherjee et al., 2021; O’Reilly & Frank, 2006; Rikhye et al., 2018). However, whether the computational agents have a correspondence not only to specific elements of the brain, but also to how the elements are connected together remains to be seen.

We also do not know the extent to which, if any, the agent architectures can account for other behaviors such as learning sequences (Cazin et al., 2019; Han et al., 2019; Zhou et al., 2020), hierarchical associations (McKenzie et al., 2014; Ribas-Fernandes et al., 2011), task switching (Hoerzer et al., 2012; Mante et al., 2013; Miconi, 2017), reversal learning (Harlow, 1949; Wang et al., 2018; Zhang et al., 2018), and other indications of schemas in learning and information processing (Baraduc et al., 2019; McKenzie et al., 2014; Zhou et al., 2020). We have also not modelled the memory consolidation (Alvarez & Squire, 1994; Kumaran et al., 2016; McClelland, 2013) result by Tse et al. (2007) in which the recall of flavor-location association pairs becomes hippocampus-independent. Future modelling should therefore explore other agent architectures. It will also be important to go beyond the rate-coded neurons we have used and implement agents with spiking neurons to enable closer comparison of model parameters with experimental observations (Brzosko et al., 2017; Frémaux et al., 2013; Zannone et al., 2018).

## Methods

### General neuron model

The membrane potential dynamics  $x_i(t)$  of all neurons, except place cells and units within the neural NAVIGATE schema, were simulated using

$$\tau \dot{x}_j(t) = -x_j(t) + \sum_{i=1}^N W_{ij} u_i(t) + \sqrt{\tau \sigma^2} \xi(t) \quad (1)$$

with membrane time constant  $\tau = 100 \text{ ms}$ , inputs  $u_j(t)$  linearly weighted using synaptic weights  $W_{ij}$  and stochasticity defined using Gaussian white noise process  $\xi(t)$  with zero mean and unit variance and tuned individually using  $\sigma$ . The firing rates are modelled using either a linear or nonlinear activation function. Each neuron's dynamics was discretized with the Euler–Maruyama method:

$$x_j(t) = (1 - \alpha)x_j(t - \Delta t) + \alpha \left( \sum_{i=1}^N W_{ij} u_i(t) + \sqrt{\frac{\sigma^2}{\alpha}} N(0,1) \right) \quad (2)$$

where  $\alpha \equiv \Delta t / \tau$  and  $N(0,1)$  is the standard normal distribution. We used a time step of  $20 \text{ ms}$  for all simulations. The specific implementation is outlined in the subsequent sections.

### Model-free reinforcement learning

The biologically plausible Actor-Critic was adapted from (Kumar et al., 2022). All agents have 49 place cells whose firing rates depend on the agent's position in the arena  $s(t)$ . The firing rate of the  $i$ th place cell is

$$u_i^{pc}(t) = \exp\left(-\frac{(s(t) - s_i)^2}{2\sigma_{pc}^2}\right) \quad (3)$$

with  $\sigma_{pc} = 0.267 \text{ m}$ , and place cells centers  $s_i$  spaced  $0.267 \text{ m}$  apart at the intersections of a regular 7-by-grid. Each cue is encoded by  $u^{cue}$ , a one-hot vector of length 18 with gain 3, for example,  $u^{cue} = [0, 3, 0, \dots]$  for the second cue. The cue and  $u^{cue}$  were constant throughout each trial, except for the working memory task in Figure 7 where the cue was presented 1 second after the start of each trial for 2 seconds, similar to the experiment by Tse et al. (2007). During the cue presentation period, place cell activity and agent actions were silenced to simulate cue presentation to the rat in the starting box with no knowledge of its position in the maze. Subsequently,  $u^{cue}$  was set to zero while place cell activity and agent actions were switched on for navigation.

The place cell activities and sensory cue were concatenated to form an input vector

$$u_i(t) = [u_i^{pc}(t), u_i^{cue}(t)] \quad (4)$$

with length  $N_{inputs} = 67$  and passed to the reservoir of recurrently connected neurons as inputs. The firing rates of the reservoir neurons are

$$r_j(t) = \phi[x_j(t)] \quad (5)$$

with the nonlinear activation function

$$f(x) = \begin{cases} 0, & x < 3 \\ x, & x \geq 3 \end{cases} \quad (6)$$

And membrane potential dynamics

$$\tau \dot{x}_j(t) = -x_j(t) + \sum_{j=1}^{N_{inputs}} W_{ij}^{inp} u_i(t) + \lambda \sum_{k=1}^N W_{jk}^{rec} \tanh [x_k(t)] + \sqrt{\tau \sigma_{res}^2} \xi(t) \quad (7)$$

with  $\lambda = 1.5$  and  $\sigma_{res} = 0.025$ . The synaptic weights  $W_{ij}^{inp}$  were drawn from a uniform distribution between  $[-1,1]$ ,  $W_{ij}^{rec}$  from a Gaussian distribution with zero mean and variance  $1/pN$  with connection probability  $p = 0.1$ .

All agents have an actor of  $M = 40$  neurons with firing rate of the  $k$ th actor neuron

$$\rho_k(t) = \text{ReLU}[q_k(t)] \quad (8)$$

With the rectified linear unit activation (ReLU) function and membrane potential  $q_k$  has dynamics

$$\begin{aligned} \tau \dot{q}_k(t) = & -q_k(t) + \beta^{control} q_i^{NAV}(t) + (1 - \beta^{control}) \sum_{j=1}^N W_{jk}^{actor} r_j(t) \\ & + \sum_{h=1}^M W_{hk}^{lateral} \rho_h(t) + \sqrt{\tau \sigma_{actor}^2} \xi(t) \end{aligned} \quad (9)$$

With  $\sigma_{actor} = 0.25$ .  $q_i^{NAV}$  is the input from the symbolic or neural NAVIGATE schema. The synaptic weights  $W_{jk}^{actor}$  linearly weight the reservoir activity.  $\beta^{control}$  determines the controls the contributions from the reservoir and the NAVIGATE schema in controlling the agent's actions.  $\beta^{control}$  takes values between 0 and 1 inclusive to be either a pure Actor-Critic or schema agent respectively.  $\beta^{control} = 0.3$ ,  $\beta^{control} = 0.4$  and  $\beta^{control} = 0.9$  were used for the navigation tasks in Figure 4, 6 and 7 respectively.  $W_{hk}^{lateral}$  was defined using

$$W_{hk}^{lateral} = \frac{w_-}{M} + w_+ \frac{f(k, h)}{\sum_h f(k, h)} \quad (10)$$

with  $f(k, h) = (1 - \delta_{kh}) e^{\varphi \cos(\theta_k - \theta_h)}$ ,  $w_+ = 1$ ,  $w_- = -1$  and  $\varphi = 20$ , connect the actor neurons into a ring attractor that smooths the agent's trajectory. The  $k$ th actor neuron represents a spatial direction  $\theta_k = 2\pi k/M$  and the action

$$a(t) = \frac{a_0}{M} \sum_k \rho_k(t) [\sin \theta_k, \cos \theta_k] \quad (11)$$

is the vector sum of directions weighted by each actor neuron's firing rate, with  $a_0 = 0.03$  translating to the agent moving at about  $0.8 \text{ ms}^{-1}$ . Agents with a critic neuron has firing rate

$$v(t) = \text{ReLU}[\zeta_k(t)] \quad (12)$$

with membrane potential dynamics

$$\tau \dot{\zeta}_k(t) = -\zeta_k(t) + \sum_{j=1}^N W_{jk}^{critic} r_j(t) + \sqrt{\tau \sigma_{critic}^2} \xi(t) \quad (13)$$

with  $\sigma_{critic} = 1^{-8}$  and  $W_{jk}^{critic}$  is the synaptic weights from the reservoir. The output of the critic  $v(t)$  and the reward  $R(t)$  in Eq. 49 define the continuous temporal difference (TD) error (Doya, 2000; Frémaux et al., 2013)

$$\delta^{DA}(t) = R(t) + \dot{v}(t) - \frac{1}{\tau_g} v(t) \quad (14)$$

and discretized according to Kumar et al. (2022)

$$\delta^{DA}(t) = R(t - \Delta t) + [v(t) - (1 + \alpha_g)v(t - \Delta t)] \quad (15)$$

with  $\alpha_g \equiv \Delta t / \tau_g$  and,  $\tau_g = 3000 \text{ ms}$  for Figures 3, 5 and 7 that did not have an obstacle and  $\tau_g = 10,000 \text{ ms}$  for Figures 4 and 6 that required the agents to navigate past an obstacle (Table 1). Synaptic plasticity of the weights onto the critic is governed by the two-factor rule

$$\Delta W_{jk}^{critic}(t) = \eta_{critic} \cdot r_j(t) \cdot \delta^{DA}(t) \quad (16)$$

with the presynaptic reservoir firing rate  $r_j(t)$  modulated by the continuous TD error (Foster et al., 2000; Sutton & Barto, 2020). Synaptic plasticity of the weights from the reservoir to the actor is governed by a three-factor rule

$$\Delta W_{jk}^{actor}(t) = \eta_{actor} \cdot r_j(t) \cdot \rho_k(t) \cdot \delta^{DA}(t) \quad (17)$$

with the outer product of the presynaptic and postsynaptic activity modulated by the TD error. The learning rates were optimized for each task using a grid search between  $10^{-6}$  to  $10^{-4}$  for the actor and between  $10^{-5}$  to  $10^{-3}$  for the critic (Table. 1).

**Table 1. Hyperparameters optimized for each task**

Task	Figure	$R$	$\tau_g$ (ms)	$\eta_{critic}$	$\eta_{actor}$	$\Omega_{Ach}$
DMP	3	5	3,000	$2 \times 10^{-4}$	$5 \times 10^{-5}$	$5 \times 10^{-4}$
Single Obstacle	goal + 4	1	10,000	$1 \times 10^{-4}$	$1 \times 10^{-5}$	$5 \times 10^{-5}$
MPA	5	5	3,000	$2 \times 10^{-4}$	$5 \times 10^{-5}$	$5 \times 10^{-5}$
MPA + Obstacle	6	1	10,000	$1 \times 10^{-4}$	$5 \times 10^{-6}$	$5 \times 10^{-5}$
MPA + Distractor	7	5	3,000	$2 \times 10^{-4}$	$1 \times 10^{-4}$	$5 \times 10^{-5}$

### *LEARN METRIC REPRESENTATION algorithm*

The firing rate of the X and Y coordinate cells follow the linear dynamics of the membrane potential

$$\tau \dot{p}_j(t) = -p_j(t) + \sum_{i=1}^P W_{ij}^{coord} u_i^{pc}(t) + \sqrt{\tau \sigma_{coord}^2} \xi(t) \quad (18)$$

Where  $\sigma_{coord}^2 = 1e - 8$  and  $W_{ij}^{coord}$  is the synaptic weights from place cells to coordinate cells. Although place cells encode spatial information, it is binned instead of a continuous representation of the environment for the agent to perform vector-based navigation. The coordinate cells are an explicit metric representation of the continuous space in the maze that the agent can use to self-localize and flexibly perform vector navigation without needing a lookup table (Bush et al., 2015; Fiete et al., 2008).

Learning a metric representation is formulated as a path integration learning problem by integrating place cell activity and self-motion information  $\hat{a}(t)$ . The self-motion information is the actual displacement of the agent in an environment after correcting for bouncing off boundaries, making it different from the action  $a(t)$  specified by the agent (Eq. 11). An agent can estimate its current coordinates by performing vector addition between its displacement in the arena and the previously estimated coordinates

$$p_j(t) = p_j(t - \Delta t) + \hat{a}_j(t) \quad (19)$$

which yields the self-consistency equation

$$p_j(t) - p_j(t - \Delta t) - \hat{a}_j(t) = 0 \quad (20)$$

if the agent performed perfect path integration to accurately estimate its current coordinates. Path integration errors can be converted into a temporal difference error

$$\delta_j^{coord}(t) = p_j(t) - p_j(t - \Delta t) - \hat{a}_j(t) \quad (21)$$

which the agent minimizes by computing an eligibility trace of the place cell activity

$$\tau_{coord} \dot{e}_i(t) = -e_i(t) + u_i^{pc}(t) \quad (22)$$

with  $\tau_{coord} = 1000 \text{ ms}$  and using the two-factor Hebbian rule by taking the presynaptic place cell activity modulated by the path integration TD error

$$\Delta W_{ij}^{coord}(t) = \eta_{coord} \cdot e_i(t) \cdot \delta_j^{coord}(t) \quad (23)$$

with  $\eta_{coord} = 0.01$ . Reducing the time constant  $\tau_{coord}$  to  $200 \text{ ms}$  and  $100 \text{ ms}$  allowed the agent to learn the metric representation though convergence was increasingly slower.

### *LEARN FLAVOR-LOCATION algorithm*

When the agent navigates around the arena and receives a reward, its current location is taken to be the goal coordinates.

The symbolic agent contains a key–value association matrix, constructed using two zero-value matrices  $K$  and  $V$  of dimensions  $50 \times 18$  and  $50 \times 3$  respectively, with the number of rows arbitrarily chosen as 50; the number of rows has to be greater than the number of associations to be stored. When the reward value is greater than zero, the cue index  $C \in \{1, 2, 3, \dots, 17, 18\}$  is determined using the argmax function which specifies the argument at which the one-hot encoded cue vector  $u^{cue}$  has a value of one. The cue index specifies the row in which  $u^{cue}$  needs to be stored in the key matrix. For example, if  $C = 2$ , the vector  $u^{cue}$  is stored in the second row of the key matrix  $K(2) \leftarrow [0, 3, 0, 0, \dots, 0]$ . The same cue index  $C$  specifies the row in which the agent’s current coordinates  $p(t) = (x, y)$  concatenated with the reward recall value of 1 needs to be stored in the value matrix  $V(2) \leftarrow [x, y, 1]$  as shown in Fig. 2B.

In the subsequent trial,  $u^{cue}$  is treated as a query and a distance-based metric

$$A(t) = \text{softmax}(\beta^{recall} u^{cue}(t) \cdot K^T) \quad (24)$$

With  $\beta^{recall} = 1$  is used to compute the memory attention weight  $A(t)$  of size 50 which specifies the probability distribution if and where the flavor cue vector  $u^{cue}$  is stored in the key matrix. A dot product between the attention weight and the value matrix

$$g(t) = A(t) \cdot V \quad (25)$$

recalls the goal coordinates and reward recall value  $[x, y, 1]$  as the vector  $g(t)$ . The reward recall value describes the accuracy of recalling the goal coordinates i.e., when the recall of goal coordinates is imperfect, recall value will be lower than 1.

If the trial ends and no reward is disbursed, the entire row of the key and value matrices corresponding to the cue index  $C$  is set to 0 to delete the cue and coordinate association i.e.,  $K(2) \leftarrow 0$  and  $V(2) \leftarrow 0$ .

Instead of a symbolic key-value matrix, three readout units from a reservoir are trained to recall the X, Y goal coordinates and recall value when it receives flavor cues as inputs. The firing rate of the goal coordinate neurons  $g_i(t)$  follows the membrane potential dynamics

$$\tau \dot{g}_i(t) = -g_i(t) + g_i^{noisy}(t) \quad (26)$$

with  $g_i^{noisy}(t)$  given by a vector sum of the reservoir activity and  $W_{ij}^{goal}$  synaptic weights

$$g_i^{noisy}(t) = \sum_{j=1}^N W_{ij}^{goal} r_j(t) + \sqrt{\tau \sigma_{goal}^2} \xi(t) \quad (27)$$

as well as the exploratory white noise with  $\sigma_{goal}^2 = 0.05$ . To form an association between the flavor cue and the agent’s coordinates, a target vector  $g_i^*(t)$  is determined according to

$$g_i^*(t) = [p_i(t), \Theta[R(t)]] \quad (28)$$

which is a concatenation of the agent’s estimated coordinates and the reward value that is transformed using the step function  $\Theta$  to be a value of one when the reward is positive and a value of zero otherwise (Eq. 34). The synaptic weights were trained either by the reward modulated least mean squares FORCE (LMS) rule (Hoerzer et al., 2012; Sussillo & Abbott, 2009) which takes the presynaptic reservoir firing activity and the vector error between the target vector  $g_i^*(t)$  and goal coordinate neurons

$$\Delta W_{ij}^{goal}(t) = \eta_{goal} \cdot r_j(t) \cdot (g_i^*(t) - g_i(t)) \cdot \Theta[R(t)] \quad (29)$$

or the reward modulated exploratory Hebbian (EH) rule (Hoerzer et al., 2012) that takes the presynaptic reservoir activity and the difference between the noisy and smooth goal neuron firing activity as postsynaptic neurons

$$\Delta W_{ij}^{goal}(t) = \eta_{goal} \cdot r_j(t) \cdot (g_i^{noisy}(t) - g_i(t)) \cdot M(t) \cdot \Theta[R(t)] \quad (30)$$

A sparse modulatory factor  $M(t)$  is computed

$$M(t) = \begin{cases} 1, & \bar{P}(t) < P(t) \\ 0, & otherwise \end{cases} \quad (31)$$

where the performance index  $P(t)$  is the negative mean squared error between the target vector  $g_i^*(t)$  and the noisy goal neuron  $g_i^{noisy}(t)$  activity

$$P(t) = - \sum_{i=1}^3 [g_i^*(t) - g_i^{noisy}(t)]^2 \quad (32)$$

and a low pass filter of the performance index is  $\bar{P}(t)$  given as

$$\tau \frac{d\bar{P}}{dt}(t) = -\bar{P}(t) + P(t) \quad (33)$$

with  $\tau = 100 \text{ ms}$ , the same as the neuronal time constant. The EH rule is considered to biologically plausible as it uses only local presynaptic and postsynaptic information while the modulatory factor is a sparse scalar value (Hoerzer et al., 2012; Legenstein et al., 2010).

Importantly, the Hebbian plasticity rule needs to be modulated by the presence of the reward so that the coordinates at which a reward is disbursed is learned as the goal coordinates. A step function  $\Theta$  is used to transform the reward value

$$\Theta[R(t)] = \begin{cases} 1, & R(t) > 0 \\ 0, & otherwise \end{cases} \quad (34)$$

so that reward modulation is 0 for negative or no rewards or 1 for positive rewards.

To delete cue specific goal association, synaptic depression is modelled using acetylcholine modulated Hebbian rule (Zannone et al., 2018) which takes the reservoir activity as the presynaptic activity, the goal readout activity as the postsynaptic activity and a constant negative scalar value as the global modulatory factor

$$\Delta W_{ij}^{goal}(t) = \eta_{goal} \cdot r_j(t) \cdot g_i(t) \cdot -\Omega_{Ach} \quad (35)$$

where a higher valued acetylcholine factor causes a faster rate of synaptic depression (Fig. 2D). The value of acetylcholine is optimized according to the task (Table 1).

### NAVIGATE algorithm

Direct heading is a simple implementation of vector-based navigation. Vector subtraction is performed between the goal and agent’s current coordinates

$$d_{j \in \{x,y\}}(t) = g_{j \in \{x,y\}}(t) - p_j(t) \quad (36)$$

to determine the direction to move towards the goal from an agent’s current position. A spatial direction that is closest to the computed vector  $d_{j \in \{x,y\}}(t)$  is chosen out of the 40 possible directions defined by the actor (Eq. 11)

$$q_i^{NAV}(t) = \text{softmax} \left( \sum_{j=1}^M K_i^{actions} d_j \right) \cdot \varepsilon(t) \quad (37)$$

to directly head towards the goal. If the recall value  $g_{j=3}(t)$  is less than the pre-set threshold value of 0.6, the output is suppressed

$$\varepsilon(t) = \begin{cases} 1, & 0.6 < g_{j=3}(t) \\ 0, & otherwise \end{cases} \quad (38)$$

otherwise, the direction of movement  $q_i^{NAV}(t)$  is passed to the actor (Eq. 9) to influence the action  $a(t)$ .

A dataset with different combinations of current  $p_j(t)$ , goal  $g_j(t)$  and reward recall values  $g_j(t)$  as input and the corresponding suppressed or unsuppressed direction of movement  $q_i^{NAV}(t)$  as output was generated using the equations 36–38. Different neural network architectures with one to two hidden layers, each with 64 to 1024 hidden units with ReLU activation function were trained using backpropagation for 20 epochs to minimize the mean squared error of the dataset. All the architectures had five input neurons corresponding to the agent’s current X and Y coordinates, recalled X and Y goal coordinates and the reward recall value, and a top layer with 40 neurons with linear activation function corresponding to the direction of movement in Eq. 11. The network that achieved one of the lowest validation errors while having low computational complexity was chosen to be the NAVIGATE neural schema. This was a network with two hidden layers each with 128 units. The synaptic weights of this network were fixed and used as a static module as the agent learned the DMP and MPA tasks.

### Learning to gate working memory

Since sensory cue is given only at the start of the trial in Figure 7, a persistent representation of the cue is necessary to learn flavor-location associations. A bump attractor has been shown to recreate the persistent working memory dynamics in the prefrontal cortex (Parthasarathy et al., 2019; Wimmer et al., 2014). The bump attractor has  $N_{bump} = 54$  neurons with firing rate given by

$$u_i^{bump}(t) = \text{ReLU}[x_i^{bump}(t)] \quad (39)$$

where the membrane potential  $x_i^{bump}(t)$  has dynamics

$$\begin{aligned}
\tau \dot{x}_i^{bump}(t) = & -x_i^{bump}(t) + \chi(t) \\
& \cdot \sum_{j=1}^{M_{cue}} W_{ij}^{inwm} u_j^{cue}(t) + \sum_{h=1}^{N_{bump}} W_{ih}^{bump} \omega[x_h^{bump}(t)] \\
& + \sqrt{\tau \sigma_{bump}^2} \xi(t)
\end{aligned} \tag{40}$$

with  $\sigma_{bump} = 0.1$  and nonlinear activation function

$$\omega(x) = \begin{cases} 0, & x < 0 \\ x^2, & 0 < x < 0.5 \\ \sqrt{2x - 0.5}, & x \geq 0.5 \end{cases} \tag{41}$$

The synaptic weight  $W_{hj}^{bump}$  is defined similarly as the lateral connectivity in the actor (Eq. 10) to connect the neurons in a ring with  $w_+ = 2$ ,  $w_- = -10$  and  $\varphi = 300$ . Since the 18 cues are encoded as a one-hot vector,  $W_{ij}^{inwm}$  is specified such that each cue activates one unit in the ring using a synaptic weight of 1 and the  $W_{hj}^{bump}$  activates two adjacent units so that a total of three neurons form a subpopulation to persistently maintain each cue information.

The gating mechanism  $\chi(t)$  controls the information flow from the sensory cues to the bump attractor by either opening the gate to update the working memory with new information or closing the gate to maintain the information persistently maintained in working memory (Lloyd et al., 2012; O'Reilly & Frank, 2006; Todd et al., 2009). There are two gating neurons, each to update or maintain working memory respectively and have the membrane potential dynamics

$$\tau \dot{\vartheta}_i(t) = -\vartheta_i(t) + \sum_{j=1}^N W_{ij}^{gate} r_j(t) + \sqrt{\tau \sigma_{gate}^2} \xi(t) \tag{42}$$

and use a SoftMax selection rule to determine the probability of selecting a particular gating action

$$p^{gate}(t) = \frac{\exp[\beta^{gate} \vartheta_i(t)]}{\sum_k \exp[\beta^{gate} \vartheta_k(t)]} \tag{43}$$

with  $\beta^{gate} = 2$  and,  $\pi_i(t) = 1$  if gating action  $i$  was chosen at time  $t$  and  $\pi_i(t) = 0$  otherwise. The gating mechanism then updates or maintains working memory by

$$\chi(t) = \begin{cases} 1, & \pi_1(t) < \pi_2(t) \\ 0, & otherwise \end{cases} \tag{44}$$

opening  $\chi(t) = 1$  or closing  $\chi(t) = 0$  information flow from the sensory cues to the bump neurons. The synaptic plasticity of the weights  $W_{ij}^{gate}$  is governed by a 3-factor temporal difference error modulated Hebbian plasticity rule

$$\Delta W_{ij}^{gate}(t) = \eta_{gate} \cdot r_j(t) \cdot \pi_i(t) \cdot \delta^{DA}(t) \tag{45}$$

using the reservoir’s presynaptic activity, gating policy as postsynaptic activity and modulated by the TD error computed by the critic with  $\eta_{gate} = 10^{-4}$  and. All synapses that were trained using the Hebbian rule were initialized to zero at the start of the simulations.

### *Task descriptions*

#### Simulation 1: Random foraging

The task was to understand how LEARN METRIC REPRESENTATION schema uses place cell activity to learn a continuous metric representation. The agent had 49 place cells and coordinate cells representing X and Y axis.

The agent moves within a spatially continuous two-dimensional square arena bounded by walls of length 1.6m with possible agent positions  $x = (\pm 0.8 m, \pm 0.8 m)$ . At the start of each trial, the agent’s current coordinate estimation was reset to zeros while its position drawn with equal probability from midpoints of the found boundary walls. The agent moves by executing time-dependent actions  $a(t)$  from a random policy that affect its velocity according to

$$\dot{s}(t) = a(t) \quad (46)$$

Using Euler’s method of discretization with time step  $\Delta t$ , this results in position updates

$$s(t + \Delta t) = s(t) + \Delta t \cdot a(t) \quad (47)$$

If the updated position ends up outside the area, the agent moves 0.01 m inwards perpendicular to the closest boundary from its last position given by  $\hat{a}(t)$ . The agent explored the maze over 20 trials for 30 seconds. Synaptic plasticity from place cells to the coordinate cells was switched on according to Eq. 23

To assess the learning of metric representation, the synaptic weights, true state coordinates and agent estimated current coordinates were plotted for trials 2, 9 and 20.

#### Simulation 2: Associating cues to coordinates

This task required the reservoir with three readout units to associate up to 50 one-hot vector cue inputs with 50 goal coordinates randomly drawn from a uniform distribution between [-1,1]. The task was split into two phases, association and recall, where the cue was persistently presented.

During the association phase, the goal coordinate concatenated with a value of one for example [0.4, -0.2, 1], was set as the target vector  $g_i^*(t)$ . Synaptic plasticity governed by either the LMS or the EH rule was switched on for five seconds. There after plasticity was switched off to determine if the network was able to maintain the learned goal coordinates for five seconds. 1 up to 50 cues were presented for association before the recall phase.

During the recall phase, the reservoir’s internal activity was reset by drawing each unit’s membrane potential from a Gaussian distribution with zero mean and variance 0.1 and the cue was presented as input to the network. The one-shot recall error was determined by taking the mean square error between the target  $g_i^*(t)$  and the readout neuron activity  $g_i(t)$ .

To delete cue specific association, the target vector was set to zeros [0, 0, 0] and synaptic plasticity was switched on for the reservoir to associate the cue input to a zero vector. The number of neurons within the reservoir was increased incrementally from 128 to 2048 to assess if the size of the reservoir affecting the one-shot learning and recall accuracy.

## Displaced match to place (DMP) task

Following Steele and Morris (1999), the task involved navigating to a single goal in the square maze described in random foraging. A goal location is randomly chosen out of 49 possible reward locations distributed throughout the maze such that the centers of possible locations are 0.2 *m* from each other or a boundary. All possible reward locations are circles with a radius of 0.03 *m*. A session constitutes of four trials where the goal remains in the same location. In the following session, a new goal location is chosen. Agents solved the task over nine sessions.

The agent is free to explore the area for a maximum duration  $T_{max}$  per trial. If it finds the reward before  $T_{max}$ , the agent remains stationary until the trial ends to model consummatory behavior. After the agent reaches the reward, a total reward value  $R = 5$  is disbursed at a reward rate  $R(t)$  defined by

$$\dot{R}_{decay}(t) = -\frac{R_{decay}(t)}{\tau_{decay}}; \dot{R}_{rise}(t) = -\frac{R_{rise}(t)}{\tau_{rise}} \quad (48)$$

$$R(t) = \frac{R_{decay}(t) - R_{rise}(t)}{\tau_{decay} - \tau_{rise}} \quad (49)$$

With  $\tau_{rise} = 100$  *ms* and  $\tau_{decay} = 250$  *ms*. When the agent reaches the reward, instantaneous updates

$$R_{rise}(t) \rightarrow R_{rise}(t) + R; R_{decay}(t) \rightarrow R_{decay}(t) + R \quad (50)$$

Are made such that  $R(t)$  integrate to  $R$ . To prevent infinitely long trials, trials in which the reward is reached before  $T_{max}$  are terminated when  $R - 1^{-8}$  of the reward has been consumed. Trials in which the reward is not reached before  $T_{max}$  are terminated at  $T_{max}$ .

Non-rewarded probe trials in this and all other tasks lasted 60 seconds and did not disburse reward even if the agent reached the correct reward location. Learning rates and TD error time constants were optimized in this and all other tasks to maximize the actor-critic agent’s learning (see Table 1 in Methods).

## Single goal with an obstacle

The actor-critic algorithm allows an agent to navigate past an obstacle for single goals (Frémaux et al., 2013), while the NAVIGATE scheme only affords direct heading. To determine if a combination of actor-critic and schema could improve an agent’s navigation capability, the task was to navigate past an obstacle to a single goal found at the center of the arena with coordinates (0,0). The goal was surrounded on three sides by an inverted U-shaped obstacle with width 0.08 *m* and length 0.6 *m*. The agent’s starting positions was constrained to either the north, east or west of the arena to remove trials which the agent could solve by direct heading. The total reward value was reduced to  $R = 1$  while following the same reward rate as in Eq. 49 The rest of the task parameters remained the same as in the DMP task.

## Multiple paired associations (MPA)

To model Tse et al. (2007), the same task parameters were used as in the DMP task and in Kumar et al. (2022) where each session comprised of six trials with each of the six possible cues were given to the agent in a random sequence. Cues were given to the agent throughout the trial while the total reward value was kept at  $R = 5$  following the reward rate disbursement in Eq. 49.

To model the effect of placing the agent in a new environment with different landmarks, each place cell’s selectivity within the maze was shuffled. For example, if place cells 1 and 2 had peak activation at coordinates (-0.2,0) and (0.5,0.6), these cells will demonstrate peak activation at coordinates (0.3,-0.4) and (-0.3,-0.7) after the shuffle in a new environment.

## MPA with an obstacle

To increase the complexity of the navigation task, an obstacle was introduced to the multiple paired association arena. The obstacle consisted of a wall with width  $0.08\text{ m}$  and length  $0.8\text{ m}$ , and two parallel walls of width  $0.08\text{ m}$  and length  $0.68\text{ m}$ . The obstacle did not cover the goal locations as in the original paired association, new paired association and new maze configuration described in Tse et al. (2007). The same task parameters were used as in the MPA task though the total reward value was kept at  $R = 1$ .

**Table 2: Possible starting positions for trials with specific FLAVOR-LOCATION pairs.**

Cues given during trial	Possible starting positions
1, 4, 5, 7, 11, 13, 14	East
3, 4, 5, 6, 8, 15, 16	North
2, 3, 6, 8, 12, 15, 16	West
1, 2, 3, 4, 7, 11, 12, 13, 15	South

To prevent the agents from reaching the goals by direct heading, the starting position of the agent was constrained to Table 2 so that the goal can only be reached by navigating past the obstacle. For example, the starting position for Cue 1 is randomly chosen to either be the east or south while starting position for Cue 2 is either the west or south.

## MPA with transient cue and distractor

To fully replicate the biological experimental conditions in Tse et al. (2007), the flavor cue was given to the agent one second after the trial started for two seconds. During this cue presentation period, the place cell activity and agent's actions were silenced to simulate the rat in the starting box with no knowledge of its position in the maze. The sensory cue was then switched off, setting the sensorial cue activity to zero and place cell activity and agent's actions switched on for navigation. The task relevant cue was not given to the agent thereafter. Instead, distractor Cues 17 and 18 were chosen randomly and presented six seconds after navigation has commenced at the frequency of  $0.2\text{ Hz}$ . The distractor was presented for one second, either once or twice within a trial.

## Code availability

The code for all our models and simulations is written in Python and is available in this GitHub repository <https://github.com/mgkumar138/schema4one>.

## Acknowledgements

We thank Hui Min Tan and Roger Herikstad for discussions. This work was supported by the following grants: Singapore Ministry of Health National Medical Research Council Open Fund-Individual Research Grant (NMRC/OFIRG/0043/2017 to A.Y.Y.T. and MOH-000962 to S-C.Y.); National University of Singapore Young Investigator Award (NUSYIA\_FY16\_P22 to A.Y.Y.T.); Singapore Ministry of Education Academic Research Fund Tier 3 (MOE2017-T3-1-002 to C.L. and S-C.Y.); Singapore Ministry of Education Academic Research Fund Tier 2 (T2EP30121-0027 to C.L.); National University of Singapore Healthy Longevity Translational Research Programme Pilot Grant (HLTRP/2022/PS-04 to A.Y.Y.T.). The computational work for this article was partially performed on the High Performance Computing resources at the National University of Singapore.

## **Author contributions**

M.G.K. performed the simulations and analyses, and drafted the paper. M.G.K., C.T., C.L., S-C.Y., and A.Y.Y.T. designed the research, discussed the findings, and revised the paper.

## **Competing interests**

The authors declare no competing interests.

## References

- Alvarez, P., & Squire, L. R. (1994). Memory consolidation and the medial temporal lobe: A simple network model. *Proceedings of the National Academy of Sciences of the United States of America*, *91*(15), 7041–7045. <https://doi.org/10.1073/pnas.91.15.7041>
- Banino, A., Barry, C., Uria, B., Blundell, C., Lillicrap, T., Mirowski, P., Pritzel, A., Chadwick, M. J., Degris, T., Modayil, J., Wayne, G., Soyer, H., Viola, F., Zhang, B., Goroshin, R., Rabinowitz, N., Pascanu, R., Beattie, C., Petersen, S., ... Kumaran, D. (2018). Vector-based navigation using grid-like representations in artificial agents. *Nature*, *557*(7705), 429–433. <https://doi.org/10.1038/s41586-018-0102-6>
- Baraduc, P., Duhamel, J.-R., & Wirth, S. (2019). Schema cells in the macaque hippocampus. *Science*, *363*(6427), 635–639. <https://doi.org/10.1126/science.aav5404>
- Bartlett, F. C., & Burt, C. (1932). Remembering: a Study in Experimental and Social Psychology. *British Journal of Educational Psychology*, *3*(2), 187–192. <https://doi.org/10.1111/j.2044-8279.1933.tb02913.x>
- Bellec, G., Scherr, F., Subramoney, A., Hajek, E., Salaj, D., Legenstein, R., & Maass, W. (2020). A solution to the learning dilemma for recurrent networks of spiking neurons. *Nature Communications*, *11*(1), 1–15. <https://doi.org/10.1038/s41467-020-17236-y>
- Bicanski, A., & Burgess, N. (2020). Neuronal vector coding in spatial cognition. *Nature Reviews Neuroscience*, *21*(9), 453–470. <https://doi.org/10.1038/s41583-020-0336-9>
- Botvinick, M. M. (2012). Hierarchical reinforcement learning and decision making. *Current Opinion in Neurobiology*, *22*(6), 956–962. <https://doi.org/10.1016/j.conb.2012.05.008>
- Brzosko, Z., Zannone, S., Schultz, W., Clopath, C., & Paulsen, O. (2017). Sequential neuromodulation of Hebbian plasticity offers mechanism for effective reward-based navigation. *ELife*, *6*, 1–18. <https://doi.org/10.7554/elife.27756>
- Bush, D., Barry, C., Manson, D., & Burgess, N. (2015). Using Grid Cells for Navigation. *Neuron*, *87*(3), 507–520. <https://doi.org/10.1016/j.neuron.2015.07.006>
- Carr, M. F., Jadhav, S. P., & Frank, L. M. (2011). Hippocampal replay in the awake state: A potential substrate for memory consolidation and retrieval. *Nature Neuroscience*, *14*(2), 147–153. <https://doi.org/10.1038/nn.2732>
- Castillo, P. E. (2012). Presynaptic LTP and LTD of Excitatory and Inhibitory Synapses. *Cold Spring Harbor Perspectives in Biology*, *4*(2), a005728–a005728. <https://doi.org/10.1101/cshperspect.a005728>
- Castillo, P. E., Weisskopf, M. G., & Nicoll, R. A. (1994). The role of Ca<sup>2+</sup> channels in hippocampal mossy fiber synaptic transmission and long-term potentiation. *Neuron*, *12*(2), 261–269. [https://doi.org/10.1016/0896-6273\(94\)90269-0](https://doi.org/10.1016/0896-6273(94)90269-0)
- Cazin, N., Llofriu Alonso, M., Scleidorovich Chiodi, P., Pelc, T., Harland, B., Weitzenfeld, A., Fellous, J.-M., & Dominey, P. F. (2019). Reservoir computing model of prefrontal cortex creates novel combinations of previous navigation sequences from hippocampal place-cell replay with spatial reward propagation. *PLOS Computational Biology*, *15*(7), e1006624. <https://doi.org/10.1371/journal.pcbi.1006624>
- Daw, N. D., Gershman, S. J., Seymour, B., Dayan, P., & Dolan, R. J. (2011). Model-based influences on humans' choices and striatal prediction errors. *Neuron*, *69*(6), 1204–1215. <https://doi.org/10.1016/j.neuron.2011.02.027>
- Dayan, P. (1993). Improving Generalization for Temporal Difference Learning: The Successor Representation. *Neural Computation*, *5*(4), 613–624. <https://doi.org/10.1162/neco.1993.5.4.613>

- Dolan, R. J., & Dayan, P. (2013). Goals and habits in the brain. *Neuron*, *80*(2), 312–325. <https://doi.org/10.1016/j.neuron.2013.09.007>
- Doya, K. (2000). Reinforcement learning in continuous time and space. *Neural Computation*, *12*(1), 219–245. <https://doi.org/10.1162/089976600300015961>
- Etienne, A. S., Maurer, R., Berlie, J., Reverdin, B., Rowe, T., Georgakopoulos, J., & Séguinot, V. (1998). Navigation through vector addition. *Nature*, *396*(6707), 161–164. <https://doi.org/10.1038/24151>
- Fiete, I. R., Burak, Y., & Brookings, T. (2008). What grid cells convey about rat location. *Journal of Neuroscience*, *28*(27), 6858–6871. <https://doi.org/10.1523/JNEUROSCI.5684-07.2008>
- Finn, C., Abbeel, P., & Levine, S. (2017). Model-Agnostic Meta-Learning for Fast Adaptation of Deep Networks. In D. Precup & Y. W. Teh (Eds.), *Proceedings of the 34th International Conference on Machine Learning* (Vol. 70, pp. 1126–1135). PMLR. <https://proceedings.mlr.press/v70/finn17a.html>
- Foster, D. J., Morris, R. G., & Dayan, P. (2000). A model of hippocampally dependent navigation, using the temporal difference learning rule. *Hippocampus*, *10*(1), 1–16. [https://doi.org/10.1002/\(SICI\)1098-1063\(2000\)10:1<1::AID-HIPO1>3.0.CO;2-1](https://doi.org/10.1002/(SICI)1098-1063(2000)10:1<1::AID-HIPO1>3.0.CO;2-1)
- Frean, M., & Robins, A. (1999). Catastrophic forgetting in simple networks: An analysis of the pseudorehearsal solution. *Network: Computation in Neural Systems*, *10*(3), 227–236. [https://doi.org/10.1088/0954-898X\\_10\\_3\\_302](https://doi.org/10.1088/0954-898X_10_3_302)
- Frémaux, N., & Gerstner, W. (2016). Neuromodulated Spike-Timing-Dependent Plasticity, and Theory of Three-Factor Learning Rules. *Frontiers in Neural Circuits*, *9*, 85. <https://doi.org/10.3389/fncir.2015.00085>
- Frémaux, N., Sprekeler, H., & Gerstner, W. (2013). Reinforcement Learning Using a Continuous Time Actor-Critic Framework with Spiking Neurons. *PLoS Computational Biology*, *9*(4). <https://doi.org/10.1371/journal.pcbi.1003024>
- Fusi, S. (2021). Memory capacity of neural network models. *ArXiv Preprint ArXiv:2108.07839*, 1–29. <https://doi.org/https://doi.org/10.48550/arXiv.2108.07839>
- Gardner, M. P. H., Schoenbaum, G., & Gershman, S. J. (2018). Rethinking dopamine as generalized prediction error. *Proceedings of the Royal Society B: Biological Sciences*, *285*(1891). <https://doi.org/10.1098/rspb.2018.1645>
- Gilboa, A., & Marlatte, H. (2017). Neurobiology of Schemas and Schema-Mediated Memory. *Trends in Cognitive Sciences*, *21*(8), 618–631. <https://doi.org/10.1016/j.tics.2017.04.013>
- Gläscher, J., Daw, N., Dayan, P., & O’Doherty, J. P. (2010). States versus rewards: Dissociable neural prediction error signals underlying model-based and model-free reinforcement learning. *Neuron*, *66*(4), 585–595. <https://doi.org/10.1016/j.neuron.2010.04.016>
- Han, D., Doya, K., & Tani, J. (2019). Self-organization of action hierarchy and compositionality by reinforcement learning with recurrent neural networks. *Neural Networks*, *129*, 149–162. <https://doi.org/10.1016/j.neunet.2020.06.002>
- Harlow, H. F. (1949). The formation of learning sets. *Psychological Review*, *56*(1), 51–65. <https://doi.org/10.1037/h0062474>
- Hausknecht, M., Li, W. K., Mauk, M., & Stone, P. (2017). Machine Learning Capabilities of a Simulated Cerebellum. *IEEE Transactions on Neural Networks and Learning Systems*, *28*(3), 510–522. <https://doi.org/10.1109/TNNLS.2015.2512838>
- Hoerzer, G. M., Legenstein, R., & Maass, W. (2012). Emergence of complex computational structures from chaotic neural networks through reward-modulated hebbian learning. *Cerebral Cortex*,

24(3), 677–690. <https://doi.org/10.1093/cercor/bhs348>

- Hopfield, J. J. (1982). Neural networks and physical systems with emergent collective computational abilities. *Proceedings of the National Academy of Sciences of the United States of America*, 79(8), 2554–2558. <https://doi.org/10.1073/pnas.79.8.2554>
- Hospedales, T. M., Antoniou, A., Micaelli, P., & Storkey, A. J. (2021). Meta-Learning in Neural Networks: A Survey. *IEEE Transactions on Pattern Analysis and Machine Intelligence*, 1–20. <https://doi.org/10.1109/TPAMI.2021.3079209>
- Howard, L. R., Javadi, A. H., Yu, Y., Mill, R. D., Morrison, L. C., Knight, R., Loftus, M. M., Staskute, L., & Spiers, H. J. (2014). The hippocampus and entorhinal cortex encode the path and euclidean distances to goals during navigation. *Current Biology*, 24(12), 1331–1340. <https://doi.org/10.1016/j.cub.2014.05.001>
- Høydal, Ø. A., Skytøen, E. R., Andersson, S. O., Moser, M. B., & Moser, E. I. (2019). Object-vector coding in the medial entorhinal cortex. *Nature*, 568(7752), 400–404. <https://doi.org/10.1038/s41586-019-1077-7>
- Humeau, Y., Shaban, H., Bissière, S., & Lüthi, A. (2003). Presynaptic induction of heterosynaptic associative plasticity in the mammalian brain. *Nature*, 426(6968), 841–845. <https://doi.org/10.1038/nature02194>
- Hwu, T., & Krichmar, J. L. (2020). A neural model of schemas and memory encoding. *Biological Cybernetics*, 114(2), 169–186. <https://doi.org/10.1007/s00422-019-00808-7>
- Ito, H. T., Zhang, S. J., Witter, M. P., Moser, E. I., & Moser, M. B. (2015). A prefrontal-thalamo-hippocampal circuit for goal-directed spatial navigation. *Nature*, 522(7554), 50–55. <https://doi.org/10.1038/nature14396>
- Ji, D., & Wilson, M. A. (2007). Coordinated memory replay in the visual cortex and hippocampus during sleep. *Nature Neuroscience*, 10(1), 100–107. <https://doi.org/10.1038/nn1825>
- Karlsson, M. P., & Frank, L. M. (2009). Awake replay of remote experiences in the hippocampus. *Nature Neuroscience*, 12(7), 913–918. <https://doi.org/10.1038/nn.2344>
- Katsuki, H., Kaneko, S., Tajima, A., & Satoh, M. (1991). Separate mechanisms of long-term potentiation in two input systems to CA3 pyramidal neurons of rat hippocampal slices as revealed by the whole-cell patch-clamp technique. *Neuroscience Research*, 12(3), 393–402. [https://doi.org/10.1016/0168-0102\(91\)90070-F](https://doi.org/10.1016/0168-0102(91)90070-F)
- Krotov, D., & Hopfield, J. (2021). Large Associative Memory Problem in Neurobiology and Machine Learning. *International Conference on Learning Representations*. <http://arxiv.org/abs/2008.06996>
- Kumar, M. G., Tan, C., Libedinsky, C., Yen, S.-C., & Tan, A. Y. Y. (2022). A nonlinear hidden layer enables actor–critic agents to learn multiple paired association navigation. *Cerebral Cortex*, 32(18), 3917–3936. <https://doi.org/10.1093/cercor/bhab456>
- Kumaran, D., Hassabis, D., & McClelland, J. L. (2016). What Learning Systems do Intelligent Agents Need? Complementary Learning Systems Theory Updated. *Trends in Cognitive Sciences*, 20(7), 512–534. <https://doi.org/10.1016/j.tics.2016.05.004>
- LaChance, P. A., Todd, T. P., & Taube, J. S. (2019). A sense of space in postrhinal cortex. *Science*, 365(6449), eaax4192. <https://doi.org/10.1126/science.aax4192>
- Langdon, R. B., Johnson, J. W., & Barrionuevo, G. (1995). Posttetanic potentiation and presynaptically induced long-term potentiation at the mossy fiber synapse in rat hippocampus. *Journal of Neurobiology*, 26(3), 370–385. <https://doi.org/10.1002/neu.480260309>
- Legenstein, R., Chase, S. M., Schwartz, A. B., & Maass, W. (2010). A Reward-Modulated Hebbian

- Learning Rule Can Explain Experimentally Observed Network Reorganization in a Brain Control Task. *Journal of Neuroscience*, 30(25), 8400–8410.  
<https://doi.org/10.1523/JNEUROSCI.4284-09.2010>
- Lever, C., Burton, S., Jeewajee, A., O’Keefe, J., & Burgess, N. (2009). Boundary Vector Cells in the Subiculum of the Hippocampal Formation. *The Journal of Neuroscience*, 29(31), 9771–9777.  
<https://doi.org/10.1523/JNEUROSCI.1319-09.2009>
- Lillicrap, T. P., Santoro, A., Marris, L., Akerman, C. J., & Hinton, G. (2020). Backpropagation and the brain. *Nature Reviews Neuroscience*, 21(6), 335–346. <https://doi.org/10.1038/s41583-020-0277-3>
- Limbacher, T., & Legenstein, R. (2020). H-Mem: Harnessing synaptic plasticity with Hebbian Memory Networks. *34th Conference on Neural Information Processing Systems, NeurIPS*.  
<https://doi.org/10.1101/2020.07.01.180372>
- Lloyd, K., Becker, N., Jones, M. W., & Bogacz, R. (2012). Learning to use working memory: a reinforcement learning gating model of rule acquisition in rats. *Frontiers in Computational Neuroscience*, 6(October), 1–10. <https://doi.org/10.3389/fncom.2012.00087>
- Lyu, C., Abbott, L. F., & Maimon, G. (2022). Building an allocentric travelling direction signal via vector computation. *Nature*, 601(7891), 92–97. <https://doi.org/10.1038/s41586-021-04067-0>
- Mante, V., Sussillo, D., Shenoy, K. V., & Newsome, W. T. (2013). Context-dependent computation by recurrent dynamics in prefrontal cortex. *Nature*, 503(7474), 78–84.  
<https://doi.org/10.1038/nature12742>
- Marr, D. (2010). Vision: A computational investigation into the human representation and processing of visual information. In *MIT Press* (Vol. 80, Issue 4). The MIT Press.  
<https://doi.org/10.7551/mitpress/9780262514620.001.0001>
- Marr, D., & Poggio, T. (1977). From understanding computation to understanding neural circuitry. *Neurosciences Research Program Bulletin*, 15, 470–488.
- McClelland, J. L. (2013). Incorporating rapid neocortical learning of new schema-consistent information into complementary learning systems theory. *Journal of Experimental Psychology: General*, 142(4), 1190–1210. <https://doi.org/10.1037/a0033812>
- McGovern, A., & Barto, A. G. (2001). Automatic Discovery of Subgoals in Reinforcement Learning using Diverse Density. *Proceedings of the Eighteenth International Conference on Machine Learning*, 361–368. <https://doi.org/10.5555/645530.655681>
- McKenzie, S., Frank, A. J., Kinsky, N. R., Porter, B., Rivière, P. D., & Eichenbaum, H. (2014). Hippocampal Representation of Related and Opposing Memories Develop within Distinct, Hierarchically Organized Neural Schemas. *Neuron*, 83(1), 202–215.  
<https://doi.org/10.1016/j.neuron.2014.05.019>
- Medina, J. F., & Mauk, M. D. (1999). Simulations of Cerebellar Motor Learning: Computational Analysis of Plasticity at the Mossy Fiber to Deep Nucleus Synapse. *The Journal of Neuroscience*, 19(16), 7140–7151.
- Miconi, T. (2017). Biologically plausible learning in recurrent neural networks reproduces neural dynamics observed during cognitive tasks. *ELife*, 6, 1–24. <https://doi.org/10.7554/eLife.20899>
- Moser, E. I., Kropff, E., & Moser, M. B. (2008). Place cells, grid cells, and the brain’s spatial representation system. *Annual Review of Neuroscience*, 31, 69–89.  
<https://doi.org/10.1146/annurev.neuro.31.061307.090723>
- Mukherjee, A., Lam, N. H., Wimmer, R. D., & Halassa, M. M. (2021). Thalamic circuits for independent control of prefrontal signal and noise. *Nature*, 600(7887), 100–104.

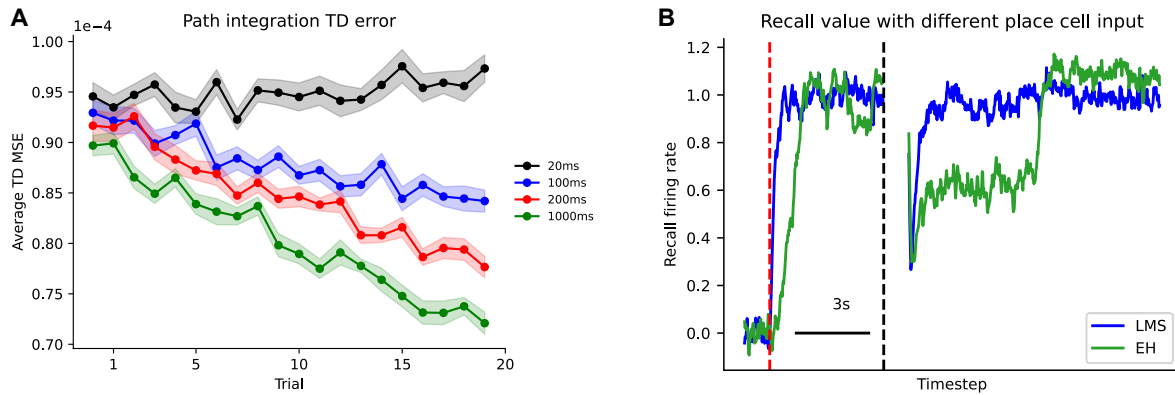
<https://doi.org/10.1038/s41586-021-04056-3>

- Müller, M., & Wehner, R. (1988). Path integration in desert ants, *Cataglyphis fortis*. *Proceedings of the National Academy of Sciences*, 85(14), 5287–5290. <https://doi.org/10.1073/pnas.85.14.5287>
- Murray, J. M. (2019). Local online learning in recurrent networks with random feedback. *ELife*, 8, 1–25. <https://doi.org/10.7554/eLife.43299>
- Nicola, W., & Clopath, C. (2019). A diversity of interneurons and Hebbian plasticity facilitate rapid compressible learning in the hippocampus. *Nature Neuroscience*, 22(7), 1168–1181. <https://doi.org/10.1038/s41593-019-0415-2>
- Nicoll, R. A., & Schmitz, D. (2005). Synaptic plasticity at hippocampal mossy fibre synapses. *Nature Reviews Neuroscience*, 6(11), 863–876. <https://doi.org/10.1038/nrn1786>
- Nyberg, N., Duvelle, É., Barry, C., & Spiers, H. J. (2022). Spatial goal coding in the hippocampal formation. *Neuron*, 110(3), 394–422. <https://doi.org/10.1016/j.neuron.2021.12.012>
- O'Reilly, R. C., & Frank, M. J. (2006). Making working memory work: A computational model of learning in the prefrontal cortex and basal ganglia. In *Neural Computation* (Vol. 18, Issue 2). <https://doi.org/10.1162/089976606775093909>
- Ormond, J., & O'Keefe, J. (2022). Hippocampal place cells have goal-oriented vector fields during navigation. *Nature*, 607(7920), 741–746. <https://doi.org/10.1038/s41586-022-04913-9>
- Parisi, G. I., Kemker, R., Part, J. L., Kanan, C., & Wermter, S. (2019). Continual lifelong learning with neural networks: A review. In *Neural Networks* (Vol. 113, pp. 54–71). Elsevier Ltd. <https://doi.org/10.1016/j.neunet.2019.01.012>
- Parthasarathy, A., Tang, C., Herikstad, R., Cheong, L. F., Yen, S.-C., & Libedinsky, C. (2019). Time-invariant working memory representations in the presence of code-morphing in the lateral prefrontal cortex. *Nature Communications*, 10(1), 4995. <https://doi.org/10.1038/s41467-019-12841-y>
- Pfeiffer, B. E., & Foster, D. J. (2015). Autoassociative dynamics in the generation of sequences of hippocampal place cells. *Science*, 349(6244), 180–183. <https://doi.org/10.1126/science.aaa9633>
- Piochon, C., Kruskal, P., MacLean, J., & Hansel, C. (2013). Non-Hebbian spike-timing-dependent plasticity in cerebellar circuits. *Frontiers in Neural Circuits*, 6(DEC), 1–8. <https://doi.org/10.3389/fncir.2012.00124>
- Poggio, T. (2012). The levels of understanding framework, revised. *Perception*, 41(9), 1017–1023. <https://doi.org/10.1068/p7299>
- Poucet, B., & Hok, V. (2017). Remembering goal locations. *Current Opinion in Behavioral Sciences*, 17, 51–56. <https://doi.org/10.1016/j.cobeha.2017.06.003>
- Ravi, S., & Larochelle, H. (2017). Optimization as a model for few-shot learning. *5th International Conference on Learning Representations, ICLR 2017 - Conference Track Proceedings*, 1–11.
- Ribas-Fernandes, J. J. F., Solway, A., Diuk, C., McGuire, J. T., Barto, A. G., Niv, Y., & Botvinick, M. M. (2011). A Neural Signature of Hierarchical Reinforcement Learning. *Neuron*, 71(2), 370–379. <https://doi.org/10.1016/j.neuron.2011.05.042>
- Rikhye, R. V., Gilra, A., & Halassa, M. M. (2018). Thalamic regulation of switching between cortical representations enables cognitive flexibility. *Nature Neuroscience*, 21(12), 1753–1763. <https://doi.org/10.1038/s41593-018-0269-z>
- Ritter, S., Wang, J. X., Kurth-Nelson, Z., Jayakumar, S. M., Blundell, C., Pascanu, R., & Botvinick, M. (2018). Been there, done that: Meta-learning with episodic recall. *35th International Conference on Machine Learning, ICML 2018*, 10(1), 6929–6938.

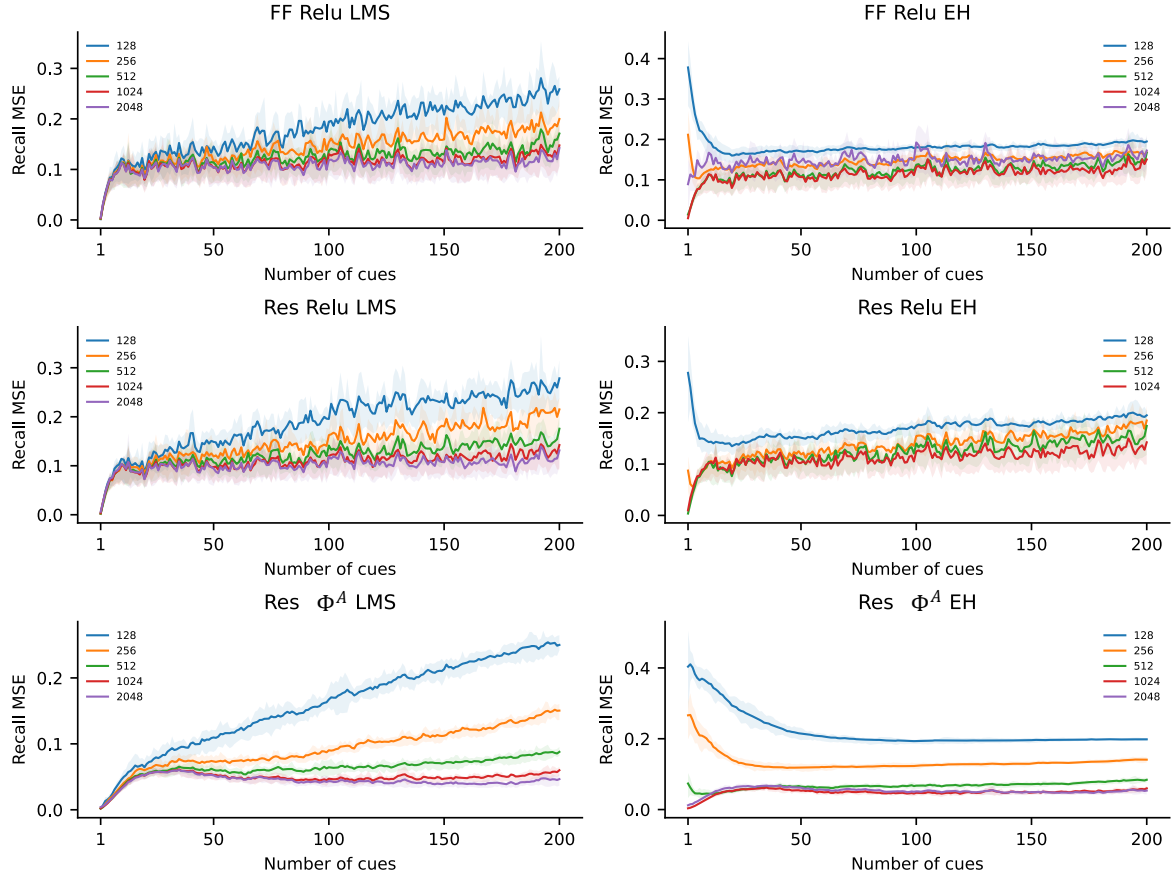
- Robins, A. (2004). Sequential learning in neural networks: A review and a discussion of pseudorehearsal based methods. *Intelligent Data Analysis*, 8(3), 301–322. <https://doi.org/10.3233/ida-2004-8306>
- Rolls, E. T. (2007). An attractor network in the hippocampus: Theory and neurophysiology. *Learning and Memory*, 14(11), 714–731. <https://doi.org/10.1101/lm.631207>
- Rolls, E. T. (2013). The mechanisms for pattern completion and pattern separation in the hippocampus. *Frontiers in Systems Neuroscience*, 7(OCT), 1–21. <https://doi.org/10.3389/fnsys.2013.00074>
- Rumelhart, D. E. (1980). Schemata: The building blocks of cognition. In *Theoretical Issues in Reading Comprehension* (pp. 33–58). Routledge.
- Rumelhart, D. E., & Ortony, A. (1977). The Representation of Knowledge in Memory. *Schooling and the Acquisition of Knowledge, January 1977*, 99–135. <https://doi.org/10.4324/9781315271644-10>
- Sarel, A., Finkelstein, A., Las, L., & Ulanovsky, N. (2017). Vectorial representation of spatial goals in the hippocampus of bats. *Science*, 355(6321), 176–180. <https://doi.org/10.1126/science.aak9589>
- Sharma, S., Chandra, S., & Fiete, I. R. (2022). *Content addressable memory without catastrophic forgetting by heteroassociation with a fixed scaffold*. <http://arxiv.org/abs/2202.00159>
- Spiers, H. J., Olafsdottir, H. F., & Lever, C. (2018). Hippocampal CA1 activity correlated with the distance to the goal and navigation performance. *Hippocampus*, 28(9), 644–658. <https://doi.org/10.1002/hipo.22813>
- Stachenfeld, K. L., Botvinick, M. M., & Gershman, S. J. (2017). The hippocampus as a predictive map. *Nature Neuroscience*, 20(11), 1643–1653. <https://doi.org/10.1038/nn.4650>
- Steele, R. J., & Morris, R. G. M. (1999). Delay-dependent impairment of a matching-to-place task with chronic and intrahippocampal infusion of the NMDA-antagonist D-AP5. *Hippocampus*, 9(2), 118–136. [https://doi.org/10.1002/\(SICI\)1098-1063\(1999\)9:2<118::AID-HIPO4>3.0.CO;2-8](https://doi.org/10.1002/(SICI)1098-1063(1999)9:2<118::AID-HIPO4>3.0.CO;2-8)
- Stentz, A. (1997). Optimal and Efficient Path Planning for Partially Known Environments. In *Intelligent Unmanned Ground Vehicles* (Vol. 1999, Issue December, pp. 203–220). Springer US. [https://doi.org/10.1007/978-1-4615-6325-9\\_11](https://doi.org/10.1007/978-1-4615-6325-9_11)
- Sussillo, D., & Abbott, L. F. (2009). Generating Coherent Patterns of Activity from Chaotic Neural Networks. *Neuron*, 63(4), 544–557. <https://doi.org/10.1016/j.neuron.2009.07.018>
- Sutton, R. S., & Barto, A. G. (2020). *Reinforcement learning: An introduction*. MIT Press.
- Todd, M. T., Niv, Y., & Cohen, J. D. (2009). Learning to use working memory in partially observable environments through dopaminergic reinforcement. *Advances in Neural Information Processing Systems 21 - Proceedings of the 2008 Conference*, 1689–1696.
- Tse, D., Langston, R. F., Takekuma, M., Bethus, I., Spooner, P. a, Wood, E. R., Witter, M. P., & Morris, R. G. M. (2007). Schemas and Memory Consolidation. *Science*, 316(5821), 76–82. <https://doi.org/10.1126/science.1135935>
- Tse, D., Takeuchi, T., Takekuma, M., Kajii, Y., Okuno, H., Tohyama, C., & Morris, R. G. M. (2011). Schema-Dependent Gene Activation. *Science*, 891(August), 891–896. <https://doi.org/10.1126/science.1205274>
- Tyulmankov, D., Fang, C., Vadaparty, A., & Yang, G. R. (2021). *Biological learning in key-value memory networks*. *NeurIPS*. <http://arxiv.org/abs/2110.13976>
- Urban, N. N., & Barrionuevo, G. (1996). Induction of Hebbian and Non-Hebbian Mossy Fiber Long-

- Term Potentiation by Distinct Patterns of High-Frequency Stimulation. *The Journal of Neuroscience*, 16(13), 4293–4299. <https://doi.org/10.1523/JNEUROSCI.16-13-04293.1996>
- van de Ven, G. M., Siegelmann, H. T., & Tolias, A. S. (2020). Brain-inspired replay for continual learning with artificial neural networks. *Nature Communications*, 11(1). <https://doi.org/10.1038/s41467-020-17866-2>
- Wang, J. X., Kurth-Nelson, Z., Kumaran, D., Tirumala, D., Soyer, H., Leibo, J. Z., Hassabis, D., & Botvinick, M. (2018). Prefrontal cortex as a meta-reinforcement learning system. *Nature Neuroscience*, 21(6), 860–868. <https://doi.org/10.1038/s41593-018-0147-8>
- Whittington, J. C. R., Muller, T. H., Mark, S., Chen, G., Barry, C., Burgess, N., & Behrens, T. E. J. (2020). The Tolman-Eichenbaum Machine: Unifying Space and Relational Memory through Generalization in the Hippocampal Formation. *Cell*, 183(5), 1249-1263.e23. <https://doi.org/10.1016/j.cell.2020.10.024>
- Wimmer, K., Nykamp, D. Q., Constantinidis, C., & Compte, A. (2014). Bump attractor dynamics in prefrontal cortex explains behavioral precision in spatial working memory. *Nature Publishing Group*, 17(3), 431–439. <https://doi.org/10.1038/nn.3645>
- Zalutsky, R. A., & Nicoll, R. A. (1990). Comparison of Two Forms of Long-Term Potentiation in Single Hippocampal Neurons. *Science*, 248(4963), 1619–1624. <https://doi.org/10.1126/science.2114039>
- Zannone, S., Brzosko, Z., Paulsen, O., & Clopath, C. (2018). Acetylcholine-modulated plasticity in reward-driven navigation: a computational study. *Scientific Reports*, 8(1), 9486. <https://doi.org/10.1038/s41598-018-27393-2>
- Zhang, Z., Cheng, Z., Lin, Z., Nie, C., & Yang, T. (2018). A neural network model for the orbitofrontal cortex and task space acquisition during reinforcement learning. *PLOS Computational Biology*, 14(1), e1005925. <https://doi.org/10.1371/journal.pcbi.1005925>
- Zhou, J., Jia, C., Montesinos-Cartagena, M., Gardner, M. P. H., Zong, W., & Schoenbaum, G. (2020). Evolving schema representations in orbitofrontal ensembles during learning. *Nature*, 590(March 2020). <https://doi.org/10.1038/s41586-020-03061-2>

## Supplementary Figures

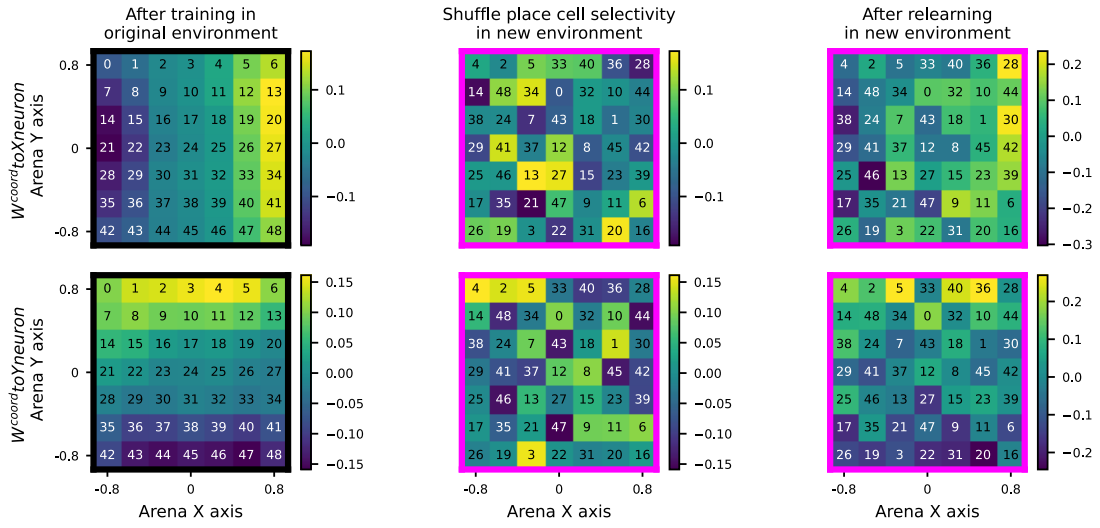


**Supplementary Figure 1. Learning LEARN METRIC REPRESENTATION and FLAVOR-LOCATION schema variables.** A) Path integration based temporal difference error decreases over 20 trials as an agent performs random foraging in an open arena for 300 seconds per trial. A longer eligibility trace time constant leads to a faster decrease in TD error. B) During navigation, the reservoir receives both sensory cue and place cell activity as input. When an agent receives a reward, plasticity is switched on and the agent's movement is restricted to associate the agent's current coordinates with the reservoir activity. During this period, place cell activity remains constant as the agent is static in the maze. When plasticity is switched on (red to black dashed lines), the reward recall value reaches 1 when either the LMS or EH rule are used. However, in the following trial when the agent is moving around the arena, causing the place cell activity to change, the recall value for the synapses trained using the LMS rule averages around 0.95 despite the changing place cell activity whereas the recall value for the synapses trained by the EH rule averages around 0.61. When the agent moves towards the goal, place cell activity becomes increasingly similar to when association occurred and the recalled reward value increases to 1.08. Hence, the reservoir trained using the EH rule activates the NAVIGATE schema when the agent gets closer to the goal while the reservoir trained using the LMS rule performs direct heading to achieve similar performance as the symbolic agent.

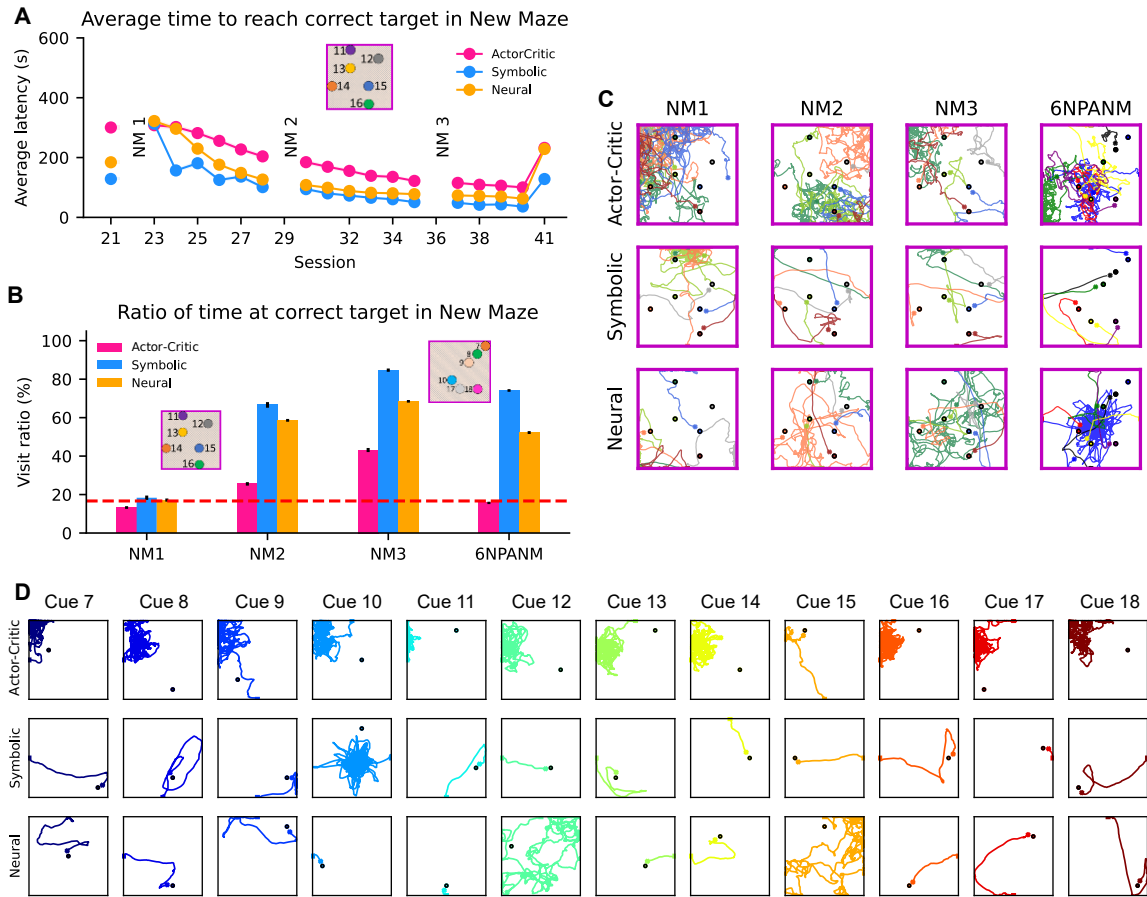


**Supplementary Figure 2. Recall error after one-shot association of multiple cue-coordinate paired associations.** The LEARN FLAVOR-LOCATION association network receives cue vector as input and passes the activity to either a feedforward (FF) or reservoir (Res) using synapses drawn from a random uniform distribution. The reservoir uses either the Rectified Linear Unit (ReLU) or the  $\Phi^A$  activation function from Kumar et al. (2022). The output are three readout units corresponding to X, Y coordinates and transformed reward value. The synapses are modified either using the LMS or EH rule. The intent is for this network to perform similarly to a key-value matrix where after forming the cue-coordinate association, when the same cue is passed to the network, the associate coordinate can be recalled with a low mean squared error (MSE). The three network architectures and two learning rules demonstrate a recall behavior where the MSE increases when the network is tasked to learn an increasing number of cue-coordinate associations. When the size of the feedforward or reservoir is increased, the recall MSE is lower. Networks trained using the LMS rule demonstrate a monotonic increase in MSE while the networks trained using the EH rule demonstrate a gradual decrease in MSE followed by a monotonic increase.

### Relearning metric representations after place cells remap



**Supplementary Figure 3. Relearning X–Y metric representation after place cells remap in a new environment.** An agent only with the LEARN METRIC REPRESENTATION schema and with synaptic plasticity turned on explored a square arena using a random policy over 20 trials for 300 seconds each. All synaptic weights were initialized to zeros before learning in the original environment (not shown). The square matrices in the top and bottom rows show the synaptic strength from place cells indexed 0 to 48 to the X and Y coordinate cells respectively. Left) After 20 sessions of random foraging in the original environment, the metric representation from the place cell population to the X (top) and Y (bottom) coordinate cells converged to represent the X axis and Y axis respectively for the agent to estimate its coordinates as described in Fig. 2A. 14 place cells with the most negative synaptic weights in the original environment are highlighted using white indices. Middle) To model place cell remapping when an animal is placed in a new environment, we randomly shuffled place cell selectivity such that place cell 0 which had peak firing activity at coordinate  $(-0.8, 0.8)$  in the original environment demonstrates peak firing activity at coordinate  $(0, 0.6)$  in the new environment. Place cell remapping leads to inaccurate coordinate estimation as the metric representation used for path integration becomes distorted. This demonstrates why the prior learned metric representation in the original environment cannot be transferred to the new environment, and a new metric representation needs to be relearned. Right) As the agent explores the new environment over 20 trials for 300 seconds each, the path integration Temporal Difference error modulated Hebbian rule gradually modifies the synaptic weights. The synaptic strength of the place cells closer to the right and left border (top row) increase and decrease, respectively to correspond to the X axis metric representation in the leftmost column. Similarly, the synaptic strength of the place cells closer to the top and bottom border (bottom row) increase and decrease, respectively to correspond to the Y axis metric representation in the leftmost column. 14 place cells with the most negative synaptic weights in the new environment are re-highlighted using white indices to demonstrate modification of synaptic weights based on the LEARN METRIC REPRESENTATION schema.



**Supplementary Figure 4. One-shot learning after gradually learning a metric representation.** A) After agents were trained on the MPA task for 20 sessions, they were introduced to the New Maze (NM) condition for another 20 sessions followed by one session of six new paired associations in the new maze (6NPANM). The NM condition was modelled where place cell selectivity was randomly shuffled so that the same place cells were now selective to a different location of the same arena and the cue-coordinate pairs followed the 6NPA condition. The actor-critic, symbolic, and neural agents gradually learn the NM and B) demonstrate increasing visit ratio performances during the probe sessions NM1, NM2, and NM3. After the agents were introduced to six new paired associations in the new maze for one session, in the subsequent probe session, the actor-critic demonstrated chance performance as it had to learn a new policy while the symbolic and neural agents demonstrated above chance visit ratio performance. This demonstrates the generalizability of the schema agents where they require several trials to gradually learn a metric representation of the new environment and can use that to demonstrate one-shot learning of new paired associations. C) Example trajectories of the actor-critic, symbolic, and neural agents during the probe sessions NM1, NM2, NM3, and 6NPANM. The actor-critic struggles to learn the new paired associates, whereas the symbolic agent navigates to all six paired associates. The neural agent navigates to five paired associates but fails to learn one PA (blue). D) Example trajectories of the three agents during a probe session after learning 12 new paired associates for a single trial each. The actor-critic navigates to the same location in the arena despite different paired associates (Cue 15). The symbolic agent fails to learn one PA (Cue 10) while the neural agent fails to learn two paired associates (Cue 12 and 15) out of 12 paired associates after a single session.